Stony Brook University

Annual Cycle and Synoptic Variability of Temperature in Great South Bay, NY

A Thesis Presented

By

Daniel Isaac Duval

to

The Graduate School

in Partial fulfillment of the

Requirements

for the Degree of

Master of Science

In

Marine and Atmospheric Science

Stony Brook University

December 2008

Stony Brook University

The Graduate School

Daniel Isaac Duval

We, the thesis committee for the above candidate for the Master of Science degree, hereby recommend acceptance of this thesis.

Dr. Robert E. Wilson
Associate Professor
School of Marine and Atmospheric Science

Dr. Charles N. Flagg
Research Professor
School of Marine and Atmospheric Science

Dr. Henry J. Bokuniewicz
Professor
School of Marine and Atmospheric Science

This thesis is accepted by the Graduate School

Lawrence Martin
Dean of the Graduate School

Abstract of the Thesis

Annual Cycle and Synoptic Variability in the Heat Balance of the Great South Bay, NY

By

Daniel Isaac Duval

Master of Science

in

Marine and Atmospheric Science

Stony Brook University

2008

A simple heat budget is created to explain the annual and synoptic scale variability of water temperature in Great South Bay, NY, balancing the vertical heat fluxes and the horizontal boundary fluxes. The hard clam *Mercenaria mercenaria* has several temperature dependencies, including spawning time, larvae survivability, and growth rate (Stanley and De Witt, 1983). Since the decline of the hard clam fishery in the late 1970s, it is important to understand all bay interactions affecting *M. mercenaria*. The boundary flux is computed two ways, indirectly by subtracting the net surface heat flux from the time rate of change of thermal energy of the bay, and directly by summing the calculated boundary fluxes, including inlet exchange (assuming total mixing), tidal residual flow, submarine groundwater discharge, and runoff, with a temperature difference ascribed to each component. On the annual scale, the net surface heat flux is dominated by shortwave radiation. Longwave and sensible heat fluxes remain nearly constant throughout the year, while latent heat flux increases during the summer as bay temperature rises. The boundary fluxes act to balance the net surface heat flux at the temperature maximum in summer and temperature minimum in winter. During spring warming and fall cooling, the boundary fluxes, which are dominated by the ocean-Bay exchange, become small due to low ocean-bay temperature difference. The agreement between the indirect boundary flux and direct boundary flux is greatest when a recirculation factor of 0.7 is introduced into the direct boundary flux calculation. This indicates that, averaged over the course of a year, 70% of water entering the bay is new ocean water and 30% is bay water ebbed on the succeeding cycle. The direct boundary flux is considered the more accurate estimate of the two boundary fluxes.

On the synoptic scale, the net surface heat flux remains the dominant mechanism for temperature change. The shortwave and longwave heat flux decreases dramatically due to high cloud cover from a frontal passage, while latent and sensible heat flux increase from increased wind stress and lower relative humidity, and higher air-Bay

temperature difference, respectively. The change in volume of the bay becomes significant, as synoptically forced winds cause coastal setup and setdown which flood and drain water from the bay. These volume changes lower the bay temperature during the summer by the input of colder ocean water dispersing the thermal energy of the bay to a larger volume. The transport of heat out of GSB from the boundary exchange can balance the net surface heat flux, but only while the latent and sensible heat fluxes are the dominant terms in the net surface heat flux.

Dedication

"If I have seen a little further it is by standing on the shoulders of Giants."
- Isaac Newton

This thesis is dedicated to my family and friends, who have given me endless support throughout my time at Stony Brook and had more faith in me than I really think I deserved at times. Sometimes the shoulders we stand on support us more than the research we produce.

Table of Contents

List of Figures

Acknowledgments

This project was funded by a New York Department of State grant awarded to Dr. Robert E. Wilson.

Many thanks to New York Department of State for funding the continuation of my education.

Very sincere thanks to my advisor, Dr. Robert E. Wilson, without whom my time here would not have been possible. He helped to plant the seed of this project in my mind and has watched it come into fruitition.

Very sincere thanks to one of my readers and mentor, Dr. Charles Flagg. His patience with my scientific bumbling has been greatly appreciated, as well as providing an endless repository for all Matlab knowledge.

Thanks to Dr. Henry Bokuniewicz for being my third reader. His perspective as a non-physical oceanographer tremendously. Additionally, I am able to graduate because I can actually pronounce his name.

Many thanks to Marianne McNamara, without whom this thesis would not have been done on time. Her harsh edits caused a dramatic improvement in the readability of this thesis, as well as helped contain the insanity of the writer.

Thanks to Tom Wilson, who on many occasions assisted with SeaCat work and provided useful information of what to do "in case something happens".

Thanks to all my fellow "first years" that came in with me, particularly Theresa, Skyler, Melissa, Tom, Santiago, Fabian, and Margaret. Theresa provided the most spectacular example of sailor-speak that would curl milk. Skyler drove herself crazy so I would not have to. Melissa invented rummy bears. Tom provided an endless supply of "that's what she said". Santiago was ok at softball, but mostly provided a good sense of humor and a funny accent. Fabian…actually not sure what he did, but things became a little less fun when he was not around. Margaret provided endless stories about how my life is not that bad, and I am by far not the most ridiculous person in the world.

Thanks to many other grad students who provided support and entertainment over the years. My Captain, Owen, those weird meteorologists, Kelly, Mike, and John, my hippy friends, Jen and Abigail, and my token Indian friend, Aleya. For those I do not mention, I still remember you, I have just run out of clever things to say. Thanks for the wild ride.

A good time was had by all.

Introduction

The Great South Bay (GSB) is a bar-built estuary situated between Long Island, N.Y. and two barrier islands, Fire Island and Jones Beach Island (Figure 1). It extends from Smith Point (-72.87 W) in the east to the beginning of the tidal marshes (-73.39 W). Approximately 40 km long and 2.5 – 8 km wide (Schubel, 1991), it extends from Smith Point (-72.87 W) in the east to the beginning of the tidal marshes (-73.39 W) in the west. GSB is extremely shallow, with an average depth of 1.8 meters (unpublished data) and an area of 235 x 10^6 m^2 (Wilson, 1991, Wong, 1981). GSB experiences exchange with the ocean through three openings; direct ocean exchange occurs through the Jones Beach and Fire Island inlets, while the easternmost part of the Bay exchanges water with Moriches Bay through Narrow Bay. Moriches Bay, in turn, exchanges with the Atlantic ocean through Moriches Inlet. There is limited exchange with South Oyster Bay in the west, but circulation is slow through that area due to numerous tidal flats that submerge during flood tide (Schubel, 1991). Tidal circulation within the bay is predominantly semidiurnal with a mean range of 58 centimeters at the Coast Guard Station in Fire Island Inlet (Wong and Wilson, 1984). Tides enter the Bay as a progressive wave, creating large tidal currents in Fire Island Inlet (1 m s-1). Tidal currents quickly attenuate within the bay due to the shallowness of the bay. Mean tidal ranges at West Islip, on the north shore of GSB, is ~30 centimeters, almost half that of Fire Island Inlet.

Previous work in GSB emphasizes the importance of synoptic scale wind forcing on bay exchange and circulation (Wong, 1981; Wong and Wilson, 1984). Wong found that Ekman forcing from longshore wind stress caused most fluctuations in coastal sea level (Wong, 1981). He also found that the inverted barometer effect cause between a fourth and a third of the variance in coastal sea level, counteracting Ekman forcing on a scale of three to seven days, and reinforcing Ekman on a scale greater than seven days. The subtidal sea level from Sandy Hook to Montauk Point could be explained by a single empirical mode, accounting for 97% of the variance, primarily forced by longshore winds (Wong and Wilson, 1984). GSB itself experienced coherent subtidal fluctuations throughout due to strong coupling with the adjacent shelf. These fluctuations caused simultaneous inflow and outflow of upwards of 20 cm s^{-1}.

Great South Bay has been the subject of intense scrutiny due to the decline of the commercially important hard clam *Mercenaria mercenaria* within the bay. Hard clam landings data provided by the New York Department of Environmental Conservation showed that harvests peaked in 1976 with over 700,000 bushels, and then dropped precipitously to less than seven thousand bushels by 2005, a harvest reduction of 99% (Figure 2). Subsequent efforts to aid in the revival of the hard clam industry have spurred research into the GSB ecosystem. Since the decline of *M. mercenaria* has continued, re-seeding projects appear to have met with limited success within the bay, indicating that a more complete view of the bay ecology is required.

Ecosystem-based management (EBM) is a concept that emphasizes the need to understand all interactions occurring within the bay before successful restoration can begin. EBM attempts to encompass every aspect of the bay that influences the species,

such as chemical, geological, biological, and physical. Chemical influences include nutrient cycling and water quality. Geological influences include bathymetry and, in the case of *M. mercenaria*, benthic habitat. Biological influences include predator-prey interactions and competitive species. Physical influences include temperature, salinity, and circulation. Additionally, EBM consists of how each aspect of the bay can influence each other (eg. biological impacts on water chemistry). This article will introduce GSB water temperature for 2007 and focus on its forcing mechanisms on an annual and synoptic scale.

Water temperature has been shown to affect both hard clam reproduction and growth rates (Stanley and De Witt, 1983; Kennedy et al., 1974). Temperature acts as a trigger for spawning, typically occurring between 22-30°C, and increases growth rates in both larval and adult hard clams. Optimum growth for hard clams occurs between 20-23°C (Stanley and De Witt, 1983). Temperature has also been shown to have an effect on the mortality rates of planktonic bivalve larvae. While temperature resistance increases with clam development, temperatures above 35°C caused 100% mortality in the early cleavage stages and trochophore larvae over periods greater than six hours (Kennedy et al., 1974). Hard clams can survive temperature ranges from <0°C to 35°C, though water pumping for food ceases in clams below 6°C and above 32°C. Beyond those ranges, survival is limited (Stanley and De Witt, 1983). Similar research done on scallops (*Pecten maximus*) show that food consumption and growth rate increased with temperature (Laing, 2000). The condition (ratio of dry meat weight to dry shell weight) of the scallops also increased with increasing temperature, with highest growth conditions occurring between 10-17°C and lowest below 8°C. While the temperature variability in GSB (-2°C – 30°C) does not exceed the temperature range of *M. mercenaria*, the clams are most affected by rapid temperature changes. For example, a 5°C increase in temperature from a nuclear power plant reduced growth in transplanted clams by over 50% (Stanley and De Witt, 1983), which will be shown to occur in GSB.

Temperature is determined by the sum of all occurring heat fluxes. The heat fluxes are not directly related to temperature, but to the first derivative of temperature. Water temperature in the bay is controlled by the net surface heat flux, and the boundary heat flux. Net surface heat flux is the combination of shortwave, longwave, latent, and sensible heat fluxes. Shortwave radiation, the amount of solar insolation that reaches the surface, is proportional to cloud cover, which blocks the incoming radiation. Longwave radiation depends on air and water temperature, relative humidity, and, most importantly, cloud cover. Increased cloud cover, occurring during synoptic scale storm events, decreases the amount of longwave radiation leaving the bay. The latent heat flux always transports energy out of the bay and depends on air temperature, water temperature, and relative humidity, and wind velocity. Latent heat flux is increases with wind speed and air temperature, which allow for greater evaporation due to turbulent convection arising from the winds and greater holding capacity as a result of warmer temperatures. Latent heat flux is inversely proportional to relative humidity, as lower relative humidities are capable of drawing more water into the air. The sensible heat flux depends primarily on the temperature difference between the air and water, and typically transports energy out of the bay. On a synoptic scale, the latent and sensible heat fluxes are expected to

become significant (Smith 1980). Large temperature drops, 4-7°C, in South Florida following frontal passages correlated strongly with increasing sensible and latent heat fluxes. The shortwave and longwave heat fluxes, while substantial, did not correlate with the daily temperature significantly. This indicates that during storms, the latent and sensible heat fluxes increase and control the water temperature.

The suitability of using routine meteorological data in the heat flux bulk formula to estimate surface heat fluxes is questionable due to the spatial distribution of sampling stations (Smith, 1985). Smith found that the surface heat fluxes are highly susceptible to wind and cloud cover. Wind data, taken from a station less than 5 km way, was shown to cause unrealistically high water temperature estimates under light wind, requiring modification of the wind record with site-specific corrections. Insolation calculated from cloud cover was also found to cause significant errors. The calculated insolation increased the standard deviation of the estimated temperature by over 1°C, from 1.94°C to 2.99°C, in comparison to pyranometer data. Smith was unable to quantify the total uncertainty in the surface heat flux calculations because the inlet exchange was neglected, but suggested the use of pyranometers and anemometers at sampling stations for the greatest accuracy.

The boundary heat flux is controlled by inlet exchange, which is comprised of tidal and subtidal oscillations, as well as tidal residual flow, submarine groundwater discharge, and runoff. The tidal oscillations are from tidal pumping, a mean tidal exchange that leaves some amount of water behind after each tidal cycle. Subtidal oscillations are, as stated previously by Wong and Wilson, due to synoptic scale wind forcing. Prevailing wind direction can cause coastal setup or set-down to occur, forcing water to flood into or drain out of the bay. Due to the multi-inlet structure of GSB, averaged over a tidal cycle, there is tidal residual flow through Jones Inlet, Moriches Bay, and South Oyster Bay which exits the bay through Fire Island Inlet (personal unpublished model data, Charles Flagg, 2008). The inlet exchange heat fluxes depend on the ocean-bay temperature difference, transporting energy into the bay in cooler months and out of the bay in warmer months.

The bay also interacts with the Bay-bottom through diffusive fluxes of heat across the water-sediment interface, which has been found to be small (Smith, 2002), and advective heat flux associated with submarine groundwater discharge. While previous estimates had shown that groundwater discharge constitutes 10-20% of the total freshwater input to the bay (Bokuniewicz, 1980), recent observation suggests that the flux of groundwater might be even greater (personal communication, Charles Flagg, 2008). Groundwater discharge has an estimated temperature of 13°C (personal communication, Henry Bokuniewicz, 2008), which is higher than the bay temperature in winter and lower than the bay temperature in summer. Groundwater discharge should also follow the same annual cycle as the inlet exchange fluxes. However, due to the unknown distribution and quantity of groundwater, its effects are, at least initially, assumed to be negligible. Runoff acts as a through flow much like the tidal residual flow and groundwater discharge. The temperature of runoff is assumed to be equal to the air temperature. The

heat flux due to runoff will then depend on the air-bay temperature difference, which is highly affected by synoptic activity.

This paper focuses on one component of EBM, the annual and synoptic scale temperature fluctuations and thermal energy balance of GSB to determine the dominate temperature forcing and the relative effect of inlet exchange. The boundary exchange will be included with the net surface heat flux in order to provide a more complete heat budget of the bay and hence the understanding of the mechanisms controlling bay temperature change. It is expected that the net surface heat flux will be balanced by the boundary flux when temperatures peak in summer and reach a minimum in winter. The net surface heat flux is also expected to control temperature change during spring heating and fall cooling with little influence from the boundary exchange.

Methods

Data Collection

Hourly-averaged bay water temperature and salinity data were collected from two stations on the north shore of GSB at Bellport (40°45'08" N 72°56'00" W) and Blue Point (40°43'20" N 73°05'197" W), NY during 2007. The data were collected using SeaBird Electronics SeaCats, model SBE-16. Hourly-averaged ocean temperature was obtained from the National Buoy Data Center (NBDC) of the National Oceanic and Atmospheric Administration (NOAA) from buoy #44017 (40°41'27" N 72°02'47" W; http://www.ndbc.noaa.gov/). Hourly-averaged water level data for Freeport and Lindenhurst, NY were obtained from the United States Geological Survey (USGS; http://waterdata.usgs.gov/nwis). Water level data for Smith Point, NY was obtained from LIShore (http://lishore.org/), though Smith Point data is missing for certain periods. The water level locations were chosen to monitor the water volume changes in GSB while minimizing the effect of along-Bay water level setup that occurs during synoptic scale storm events. The water level for the bay was calculated by averaging the three stations. When Smith Point data was missing, the average was taken between the Lindenhurst and Freeport stations. Air temperature, relative humidity, cloud cover, air pressure, wind speed and direction were obtained from the National Climatic Data Center (NCDC) of NOAA at the Islip, NY airport station, 5 kilometers north of GSB (http://cdo.ncdc.noaa.gov/qclcd/QCLCD). Incoming shortwave data was collected aboard a ferry traversing Long Island Sound from Port Jefferson, NY to Bridgeport, CT. Due to the proximity between stations, it is assumed that, on the scale of GSB, atmospheric conditions are spatially uniform.

Data Analysis

The temperature of the bay is controlled by heat flux into and out of the bay. The time rate of change of heat in the bay is a flux of thermal energy in or out of the bay

$$\frac{dH}{dt} = (Q)(A) + B_F \qquad (1)$$

i ii iii

(i) The time rate of change of thermal energy of the bay.
(ii) Net surface heat flux.
(iii) Boundary heat flux.

The thermal balance equation can be decomposed into individual terms.

i ii

$$\rho C_p V\left(\frac{\partial T_b}{\partial t}\right) + \rho C_p T_b\left(\frac{\partial V}{\partial t}\right) =$$

$$QA + \rho C_p T_I\left(\frac{\partial V}{\partial t}\right) + \rho C_p Q_T\left(T_O - T_B\right) + \rho C_p Q_G\left(T_G - T_B\right) + \rho C_p Q_R\left(T_R - T_B\right) \qquad (2)$$

iii iv v vi vii

(i) The time rate of change of thermal energy of the bay due to temperature change.
(ii) The time rate of change of thermal energy of the bay due to change in volume.
(iii) The net surface heat flux.
(vi) Inlet exchange from tidal and subtidal oscillations. T_I is the temperature of the inlet.
(v) The tidal residual heat flux. Q_T is the tidal residual flow. T_O is the ocean temperature.
(vi) Submarine groundwater discharge. Q_G is the groundwater flux. T_G is the groundwater temperature.
(vii) River flow and runoff. Q_R is the river and runoff flux. T_R is the river and runoff temperature.

Typically, the volume component of the time rate of change of thermal energy is ignored in most calculations, with the assumption that the change in temperature component is greater. Our model included both components, on the assumption that the volume component might be significant. The temperature component describes energy gained from the import of warmer ocean water or energy loss from the import of cooler ocean water. The volume component describes energy lost/gained from changing bay volume due to tidal or synoptic forcing. The net surface heat flux was estimated using the shortwave radiation data and heat flux bulk formula using atmospheric data and GSB temperature. Longwave heat flux was calculated using Fung's bulk formula (Fung, et al., 1984), while the latent and sensible heat fluxes were calculated using Fairall's bulk formula (Fairall et al., 1996).

The subtidal and tidal oscillations will be represented by term **iv**, while the tidal residual flow component of the inlet exchange will be represented by term **v**. Model output has previously estimated the tidal residual flow for GSB to be ~90 $m^3\ s^{-1}$ (unpublished model data, Charles Flagg, 2008). Groundwater discharge is estimated at

2.5 m^3 s^{-1} and river flow and runoff flow is estimated at 12.5 m^3 s^{-1} (Bokuniewicz, 1980). The temperature of the inlet is estimated assuming total mixing on flood tide and ebb tide. During flood tides the temperature of the inlet is equal to the ocean temperature, while during ebb tides the temperature is equal to the bay temperature. The area of the bay is assumed to be constant, so the time rate of change of volume can be broken down.

$$\frac{dV}{dt} = A\frac{\partial \zeta}{\partial t} \tag{3}$$

ζ is the spatially averaged water level of the bay. By entering (3) into (2), the thermal balance equation has units of watts per square meter.

i **ii**

$$\rho C_p (h+\zeta)\left(\frac{\partial T_B}{\partial t}\right) + \rho C_p T_B \left(\frac{\partial \zeta}{\partial t}\right) =$$

$$Q + \rho C_p T_I \left(\frac{\partial \zeta}{\partial t}\right) + \rho C_p \left(\frac{Q_T}{A}\right)(T_O - T_B) + \rho C_p \left(\frac{Q_G}{A}\right)(T_G - T_B) + \rho C_p \left(\frac{Q_R}{A}\right)(T_R - T_B) \tag{4}$$

iii **iv** **v** **vi** **vii**

For terms **v**, **vi**, and **vii**, the area is estimated at 235 x 10^6 m^2 with a mean water depth (h) of 1.8 meters derived from previous research (unpublished data). The boundary heat flux will be estimated using two methods. First, the indirect boundary heat flux will be estimated by subtracting the net surface heat flux from the time rate of change of thermal energy in the Bay. Secondly, the direct boundary heat flux will be estimated by calculating the sum of the four defined boundary heat flux terms (**iv**-**vii**).

$$BFd = \rho C_p (h+\zeta)\left(\frac{\partial T_B}{\partial t}\right) + \rho C_p T_B \left(\frac{\partial \zeta}{\partial t}\right) - Q \tag{5}$$

$$BFt = \rho C_p T_I \left(\frac{\partial \zeta}{\partial t}\right) + \rho C_p \left(\frac{Q_T}{A}\right)(T_O - T_B) + \rho C_p \left(\frac{Q_G}{A}\right)(T_G - T_B) + \rho C_p \left(\frac{Q_R}{A}\right)(T_R - T_B) \tag{6}$$

The two time scales of interest are the annual scale and synoptic scale. Data for the annual scale will be filtered at 30 days, removing any synoptic scale variability and focusing on long term forcing. The synoptic scale data will mostly remain unfiltered. Certain data, such as the net surface heat flux, will be filtered at 48 hours to remove diurnal and semi-diurnal forcing. This is due to the large diurnal variations, especially with the shortwave radiation. Filtering does cause uncertainty in the beginning and end of the records. For this reason, the first and last 7 days in the annual record and the first and last 7 hours in the synoptic scale will be ignored.

Results

Both temperature records follow the same pattern with limited differences (Figure 3). Additional stations are equally coherent and follow the same trend (Figure 4). The diurnal variations in temperature are small, typically less than 1°C, compared to the synoptic scale (2-10 day) variability, typically at least 3-4°C. Since the temperature records across the bay are visually coherent, the bay temperature is estimated by averaging the Bellport and Blue Point records. The temperature coherency is in great contrast to the salinity record at these stations during the same period (Figure 5). The Bellport station is highly sensitive to salinity change during wind driven events due to its location near Narrow Bay (Figures 6,7). The Blue Point station is likely insensitive to salinity change due to its location at one of the widest spots in GSB and lack of nearby fresh or saltwater sources.

Annual Scale

The mean annual temperature range of GSB is -1°C to 30°C (Figure 3). The bay and air temperature records are in phase, both beginning to warm in February (Figure 8). The ocean temperature lags in March, however, and does not warm up until mid-April. Ocean temperature is in phase with the air and bay records in early August, when all three signals peak. Temperatures then drop almost immediately, reaching ~2.5°C in December. The largest rate of change of temperatures occurs from March to June (~7°C per month) and October to December (~8°C per month). GSB warms more slowly and over a longer period of time than it cools. On the annual scale, air temperature is always cooler than the Bay by 1 to 5°C while the ocean temperature is ~5°C warmer than the bay from mid-November to March and 3-5°C cooler than the bay from mid-April to October.

The controlling factor in the net surface heat flux is shortwave radiation. Shortwave radiation increases as early as February, peaks in the beginning of July, and decreases starting in August, in part due to cloudiness caused by synoptic scale storm events (Figure 9). A sharp decline occurs during September and October, and reaches a minimum in December. Longwave radiation remains fairly constant throughout the year with little variation, indicating that synoptic scale events have little effect on the annual longwave cycle. The latent heat flux increases in magnitude with rising water temperatures (Figure 10). The magnitude of sensible heat flux is small compared to other terms, but constantly transports energy out of the bay, reaching a maximum in February when the air-bay temperature difference is greatest.

The time rate of change of thermal energy mimics the temperature component (Equation 3, Term **i**; Figure 11). The temperature component has a seasonal cycle; positive in spring months when the bay is warming, negative in fall months when the bay is cooling, and near zero during the peak of summer and winter months. The volume component (Equation 3, Term **ii**) is not entirely negligible on an annual scale. During June and October the volume component has a larger magnitude than temperature. For most of the year, however, the temperature component dominates the time rate of change

of thermal energy. Unlike the temperature component, the volume component has no apparent periodicity.

The indirect boundary flux mirrors the net surface heat flux, since the magnitude of the net surface heat flux is much larger than the time rate of change of thermal energy (Figure 12). The indirect boundary flux then follows an annual cycle as well, transporting energy into the bay in winter and out of the bay in summer at a similar magnitude as the net surface heat flux. Assuming 2007 is representative of a true annual cycle of GSB, neither the net surface heat flux nor the indirect boundary flux has a sinusoidal annual cycle, as their peaks are ill-defined. The energy transport into the bay by the indirect boundary flux reaches a maximum in December and remains ~40 W m^{-2} until February. The indirect boundary flux then decreases, reaching a maximum energy transport out of the bay in May and remains ~100 W m^{-2} through July before increasing. The net surface heat flux follows the same pattern in reverse, reaching a maximum in May that continues through July. The net surface heat flux minimum occurs in November and continues through mid-February.

The tidal and subtidal, tidal residual flow and groundwater discharge follow an annual cycle, transporting thermal energy into the bay in winter and out of the bay in summer, while runoff transports energy out of the bay year round (assuming that runoff occurs at approximately air temperature; Figure 13). However, the flux of water involved with the tidal residual flow, groundwater, and runoff is small in comparison to the volume of the bay, so that thermal energy transported is small. Compared to heat flux due to tidal and subtidal oscillations, the heat flux due to tidal residual flow, groundwater discharge, and runoff are negligible. Therefore, the direct boundary flux is dominated by tidal and subtidal oscillations. These oscillations, in turn, is controlled by the temperature of the inlet and the time rate of change of volume of the bay.

Synoptic Scale

Synoptic scale wind events are caused by the passing of low pressure systems, typically from Canada (Austin and Lentz, 1999), and have a large impact on Bay temperature, in some cases altering the temperature by over 5°C in less than a week. From September 11th to 19th, the bay drops ~6°C recovering 4°C from September 19th to 22nd (Figure 14). This drop in bay temperature is accompanied by a 15°C drop in air temperature. From air pressure and cloud cover data, this drop in air temperature is due to the passage of two low pressure systems (Figure 15), the first occurs on September 12th, the second occurring on September 15th. Both systems are characterized by high cloud fractions and increased precipitation. Shortwave and longwave radiation decrease in magnitude before the low pressure system reaches GSB, beginning September 10th (Figure 16), when the cloud fraction is increasing, and recover when the cloud fraction decreases on September 12th. The magnitude of the latent heat flux decreased at the same time as shortwave and longwave radiation, but increases more quickly and becomes larger than average before decreasing to the average. Sensible heat flux increases with the air-bay temperature difference. The first synoptic event will be the focus of the synoptic scale analysis, due to missing data in the net surface heat flux during the second

synoptic event. As with the annual scale, the filtering mechanism causes uncertainty in the beginning and end of the record. The first and last 7 hours of the filtered records will be ignored.

The time rate of change in thermal energy of the bay operates in concert with the volume component (Figure 17). Before the September 12th event, the volume component drops dramatically while the temperature component slowly starts to decrease. Beginning September 11th, the volume and temperature components act inversely. The volume component rebounds, becoming largely positive (>150 W m^{-2}), while the temperature component reaches a minimum (~-100 W m^{-2}) on September 12th. The temperature component then begins to recover while the volume component decreases rapidly. Complete recovery of the temperature component does not occur due to the second synoptic event. The volume and temperature components are inversely related during the second synoptic event as well.

Discussion

The earlier assumptions that submarine groundwater discharge was negligible and the volume component of the time rate of change of thermal energy was not negligible proved to be correct (Figures 9,13). Submarine groundwater discharge provided a minimal flux of thermal energy into GSB in comparison to the tidal and subtidal oscillations term (Equation 4, Term **v**). Even if the flux of groundwater is larger than estimated, at 2.5 m^3 s^{-1}, it would have to be two orders of magnitude greater before it would have an effect comparable to tidal and subtidal oscillations (Figure 18). The volume component of the time rate of change of thermal energy was non-trivial. On the annual cycle the volume component was fairly small although there were times when it was comparable with the temperature component. On the synoptic scale the volume component had a larger impact on the time rate of change of thermal energy. Thus, groundwater discharge can be neglected, while, depending on the time scale, the volume component cannot.

The lack of coherency between salinity and temperature (Figures 3,5) indicates that the forcing mechanisms for the two parameters are different. Salinity is controlled primarily through exchange between the ocean and bay, since freshwater input is small compared to tidal and subtidal oscillations. Temperature was hypothesized to be forced primarily by local atmospheric heating and cooling. This is not entirely accurate, as the volume component balances the net surface heat flux, particularly during the summer and winter. The net surface heat flux dominates the temperature record in spring and fall when the ocean-bay temperature difference is small.

Annual Scale

The indirect boundary flux and direct boundary flux are similar in magnitude and follow the same annual pattern (Figure 19). Both boundary heat fluxes transport energy out of the bay during the summer and into the bay during the winter. There are two major differences in the boundary heat flux estimates. First, at the beginning of March,

the indirect boundary flux drops to zero, transporting no energy in or out of the bay, despite the ocean remaining 4°C warmer than the bay (Figure 20). Similarly, in the fall, the indirect boundary flux becomes zero in mid October, while the ocean is ~1°C cooler than the bay. In both cases, the indirect boundary flux should transport energy into and out of the bay, respectively. The direct boundary flux follows the expected pattern, transporting no energy in or out of the bay when the ocean and bay waters are the same temperature (Figure 21). Secondly, the direct boundary flux is ~100 W m^{-2} larger than the indirect boundary flux during the winter and ~50 W m^{-2} lower than the indirect boundary flux in the summer.

The disparity in the two fluxes can be explained by uncertainty involved in the calculations. The indirect boundary flux has three potential sources of uncertainty, instrumental, surface heat flux bulk formula, and the assumption of spatial homogeny in the atmospheric data. Uncertainty in instrumental measurements is typically considered negligible from instrumental specifications. The bulk formula, designed for open ocean heat fluxes, carry some uncertainty as well. The assumption that atmospheric conditions are spatially uniform across GSB is not necessarily valid. Wind and cloud cover can have large spatial variations, which will in turn affect the bulk formula. Unfortunately, these uncertainties cannot currently be accounted for. The bulk formula, while not exact, provides the best estimate for the surface heat fluxes. Moreover, there are no meteorological stations closer to our study area than Islip airport. It is highly unlikely, however, that these errors could entirely account for the entirety of the disparity between the indirect boundary flux and direct boundary flux.

Similarly, the direct boundary flux also has three potential sources of uncertainty, instrumental uncertainty, a missing boundary heat flux term, and the assumption of total tidal mixing. As noted earlier, the uncertainty due to instrumental error is typically assumed to be negligible. A missing boundary flux term that would transport of energy out of the bay in the winter would require GSB interacting with a thermal reservoir with lower heat content that has yet to be identified. Conversely, during the summer, that thermal reservoir would have to have higher heat content than GSB to transport energy into the bay. There is no known thermal reservoir that acts as described, and hence no missing boundary flux. Total mixing between GSB and ocean waters during flood and ebb tides, however, do not necessarily occur. Alongshore currents and winds will cause ebbed waters to be moved away from the inlet, allowing the water on the following flood tide to be composed of completely new water. Otherwise, water could pile up outside the inlet and be recirculated into the bay during the following flood tide. Using Fisher's model (Fischer et al. 1979), it is assumed that there is non-total mixing both inside and outside the bay. Term **iv** of equation four then becomes $\rho C_p\left(\alpha T_o + (1-\alpha)T_B\right)\left(\frac{\partial \zeta}{\partial t}\right)$ when the bay floods and $\rho C_p\left(\alpha T_B + (1-\alpha)T_O\right)\left(\frac{\partial \zeta}{\partial t}\right)$ when the bay ebbs, where α represents a mixing ratio between ebbed Bay and ocean waters Alpha values ranging from 0.05 to 1 were tested at intervals of 0.05 to see which caused the best fit between the indirect boundary flux and direct boundary flux. The best fit was obtained by taking the variance between the direct boundary flux and indirect boundary flux at each alpha value.

$$\Sigma\left[\frac{(BFt - BFd)^2}{n-1}\right] \quad (7)$$

When the variance is plotted against alpha, the least variance occurs at 0.7 (Figure 22). This indicates that, averaged over a year, the water flooded into the bay is 70% new ocean water and 30% recirculated bay water, or that 70% of the ocean water is retained in GSB. Using this estimated recirculation factor, the two boundary heat fluxes become more consistent with each other (Figure 23), although the direct boundary flux is continuously higher than the indirect boundary flux. The lower indirect boundary flux could be due to a high bias in the calculation of the net surface heat flux. The assumption of spatially uniform atmospheric data and uncertainty in the use of open ocean heat flux bulk formula could estimate a higher lower heat flux than is actually experienced, causing the indirect boundary flux to be lower. Comparatively, the direct boundary flux is likely more accurate than the indirect boundary flux due to less uncertainty in its calculation.

Synoptic Scale

During the September 11th to 19th synoptic event, the direct boundary flux mimics the volume component of the time rate of change of thermal energy, indicating that the change in volume of the bay on the synoptic scale can alter the bay temperature response (Figure 24). The boundary heat flux does not dominate the temperature response, but works in conjunction with the net surface heat flux.

Cloud cover reduces the amount of insolation reaching the surface, as well as decreases the magnitude of the longwave heat flux (Figures 15,16). As suggested by Smith, the latent and sensible heat fluxes increase following the passage of the synoptic event (Smith, 1980). Before the synoptic event occurs, the high moisture content of the air causes a decrease in latent heat flux. After it rains, the latent heat flux rebounds since either much of the moisture has been precipitated out or the air is replaced by dryer continental air. Sensible heat flux out of the bay increases due to the air-water temperature difference increase from cooler air brought in by synoptic events. The net surface heat flux becomes negative during this time, transporting energy out of the bay, and causing the temperature to decrease. Immediately following the synoptic event the shortwave heat flux recovers, but the net surface heat flux remains low due to an increase in magnitude of the longwave and latent heat fluxes. The magnitude of the longwave heat flux increases as cloud cover left the area, and the magnitude of the latent heat flux increases since the air lost moisture from precipitation.

The volume component (Equation 3, Term **ii**) of the time rate of change of thermal energy of the bay becomes significant as the change in volume is comparable to the change in temperature. Since the change in volume becomes so large, the boundary heat flux mimics the volume component (Figure 24) and, despite superficially adding energy to the bay, can have an inverse impact on temperature by transporting cooler ocean water into the bay. The boundary heat flux, while adding energy through increased volume, negatively affects the temperature since the ocean water transported into the bay

has a lower temperature. The ocean water mixes with bay water, causing a dispersal of the heat content to a larger volume. When the volume decreases, the water leaving the bay has more energy than when it entered the bay, causing a heat loss. The volume changes driving the boundary flux are caused by wind forcing. Winds prior to September 7 were predominately from the southeast (Figure 7), causing a coastal set-up that caused water to flood into the bay, increasing the bay volume. After September 7th, the winds shifted to the southwest. These continuous winds caused a coastal set-down, causing the bay to drain. On September 10th a wind shift occurred, causing winds from the southeast, again causing a coastal setup that transported cooler ocean water to flood into the bay.

Despite large variability in the volume component of the time rate of change of thermal energy and the direct boundary flux, the change in temperature appears largely dominated by the net surface heat flux (Figure 25). The temperature component of the time rate of change of thermal energy mimics the net surface heat flux. The net surface heat flux is larger at most times, indicating that the boundary flux does transport heat out of the bay through the dispersion mechanism described above. The net surface heat flux becomes positive on September 13th, but the time rate of temperature is still negative due to the boundary exchange causing a net heat flux out of the bay. Unfortunately, due to missing data, the net surface heat flux response during the second synoptic event on September 15th cannot be seen.

Bay temperature begins to recover beginning September 19th. At this time, despite the boundary flux still being active, its effects are minor because the ocean-bay temperature difference at this time is ~0°C. At this point the net surface heat flux, already positive, begins increasing as sensible, latent, and longwave heat fluxes decline. Since the boundary flux is no longer transporting energy out of the bay and the net surface heat flux is increasing, the bay begins to warm. This recovery continues until September 22nd, when another synoptic event occurs.

The September 11th to 19th synoptic event may not be typical of all events. While a similar pattern occurs during the September 23rd synoptic event, it can be altered by two major factors, ocean-bay temperature difference and storm track. During winter months when the ocean is warmer than the bay, the same mechanism described would act to transport heat into the bay, increasing the temperature. The track of low pressure systems alters the wind field which affects the water level response. Since the volume component is a dominant factor in both the direct boundary flux and time rate of change of thermal energy, changing the water level response would change how the temperature responds.

While annual scale bay temperature never exceeded the preferred temperature range of *M. mercenaria*, synoptic scale events could negatively impact the species growth and development. Spawning of *M. mercenaria* typically occurs from May to August (Stanley and De Witt, 1983), when the ocean-bay temperature difference is at least 4°C. Synoptic events occurring during spawning times could change bay temperature rapidly enough to cause mortality in the hard clam planktonic larvae or transport the larvae out of the bay entirely, exposing the larvae to the colder ocean water.

Conclusions

The time rate of change of thermal energy, net surface heat flux, and boundary exchange of GSB all have varying effects depending on the time scales involved. On an annual scale, the time rate of change of thermal energy in the bay is dominated by the temperature component (Equation 3, Term **i**). The boundary heat flux is dominated tidal and subtidal oscillations. Since the time rate of change of thermal energy is largely temperature-dependent, the impact of tidal and subtidal oscillations on an annual scale is driven by the temperature difference between the ocean and the bay. The net surface heat flux is controlled by the incoming shortwave radiation, though the longwave, latent, and sensible heat fluxes can alter the magnitude. When the temperature peaks in winter and summer, the boundary heat flux, primarily tidal exchange, balances the net surface heat flux, causing the time rate of change of thermal energy in the bay to become near zero. During the spring and fall, the boundary heat flux becomes relatively small, as the temperature of the bay equals that of the ocean, and the net surface heat flux dominates. The direct calculation of the boundary flux is likely the more accurate of the two estimates, and has a recirculation factor of 30%, meaning 30% of the water flooded into the bay is old bay water from the previous ebb.

During synoptic events, despite large volume changes occurring due to synoptic wind forcing, the net surface heat flux is the dominant forcing mechanism for bay heating and cooling. Due to the large volume changes, both the volume component (Equation 3, Term **ii**) of the rate of change of thermal energy and the boundary heat flux become volume-dependent. The volume component becomes comparable to the temperature component, but does not have a large impact on the rate of change of temperature. The boundary flux is not insignificant, and can balance the net surface heat flux by the dispersal of thermal energy from the flooding of cool ocean water in and the draining of bay water out.

There are improvements that can be made to increase the accuracy of the results. In order to minimize errors in the calculations, meteorological stations should be installed with water instruments so that the assumption of no spatial variability in atmospheric data would not be required. In addition, more stations should be placed on the south shore of GSB, to insure that the estimated bay temperature is as accurate as possible. An instrument should also be placed within the inlets, so that a more accurate estimate can be made of recirculation, which would increase the accuracy of the oscillations term. This is especially important since increased storm activity can increase or decrease the mixing outside the inlet, depending on the prevailing wind directions.

This suggests that the bay temperature is difficult to alter. While on an annual scale the boundary flux balances the net surface heat flux during the warmest and coldest parts of the year, on a synoptic scale it helps cause dramatic shifts in bay temperature. The boundary flux could be decreased, possibly by closing an inlet, to lessen the severity of synoptically forced temperature change. This could also decrease the boundary exchanges ability to balance the net surface heat flux, causing the bay to get hotter in the summer, possibly beyond the survivable range of *M. mercenaria*, and colder in the

winter, stressing the *M. mercenaria* further. If the boundary flux is increased to lower the bay temperatures in the summer closer to the temperature at which *M. mercenaria* experiences the largest growth, bay temperature changes caused by synoptic events could also increase, either in duration or in magnitude. Additional research needs to be done, particularly in terms of GSB circulation modeling, in order to understand the effect of altering the boundary flux could have on the bay and hard clam survival.

Literature Cited

Smith, N. 2002. Observations and Simulations of Water-sediment Heat Exchange in a Shallow Coastal Lagoon. Estuaries. Vol. 25; pp:483-487.

Laing, Ian. 2000. Effect of temperature and ration on growth and condition of king scallop (*Pecten maximus*) spat. Aquaculture. Vol. 183; pp:325-334.

Austin, J.A., Lentz, S.J. 1999. The relationship between synoptic weather systems and meteorological forcing on the North Carolina inner shelf. Journal of Geophysical Research. Vol. 104; No. C8; pp:18159-18185.

Fairall, C.W., Bradley, E.F., Rogers, D.P., Edson, J.B., Young, G.S. 1996. Bulk parameterization of air-sea fluxes for Tropical Ocean-Global Atmosphere Coupled-Ocean Atmosphere Response Experiment. Journal of Geophysical Research. Vol. 101; No. C2; pp:3747-3764.

Wilson, R.E., Wong, K.C., Carter, H.H. 1991. Aspects of Circulation and Exchange in Great South Bay. In: Schubel, J.R., Bell, T.M., Carter, H.H. (eds). The Great South Bay. State University of New York Press, Stony Brook, NY. pp:9-22

Smith, N. 1985. The Suitability of Routine Weather Data for Estimating Local Estuarine Heat Energy Fluxes. Estuaries. Vol. 8; No. 3; pp:270-278.

Wong, K.C., Wilson, R.E. 1984. Observations of Low-Frequency Variability in Great South Bay and Relations to Atmospheric Forcing. Journal of Physical Oceanography. Vol. 14; pp: 1983-1900.

Fung, I.Y., Harrison, D.E., Lacis, A.A. 1984. On the Variability of the Net Longwave Radiation at the Ocean Surface. Reviews of Geophysics and Space Physics. Vol. 22; No. 2; pp:177-193.

Stanley, J.G., DeWitt, R. 1983. Species Profiles: Life Histories and Environmental Requirements of Coastal Fishes and Invertebrates (North Atlantic). Hard Clam. Fish and Wildlife Service. FWS/OBS-82/ 11.18. U.S. Army Corps of Engineers, TR EL-82-4.

Wong, K.C. 1981. Subtidal volume exchange and the relationship to meteorological forcing in Great South Bay, New York. PhD dissertation, Marine Science Research Center, Stony Brook University, 230 pp.

Smith, N.P., Kierspe, G.H. 1980. Local Energy Exchanges in a Shallow, Coastal Lagoon: Winter Conditions. Estuarine Coastal Marine Science. Vol. 13; pp159-167.

Bokuniewicz, H. 1980. Groundwater Seepage into Great South Bay, New York. Estuarine and Coastal Mar. Sci. Vol. 10; pp:437-444.

Fischer, H., List, E., Koh, R., Imberger, J., Brooks, N. Mixing in Inland and Coastal Waters. Academic Press, Inc. ©1979

Kennedy, V.S., Roosenburg, W.H., Castagna, M., Mihursky, J.A. 1974. *Mercenaria mercenaria* (Mollusca: Bivalvia): Temperature-Time Relationships for Survival of Embryos and Larvae. Fishery Bulletin, U.S. Vol. 73; pp:1160-1166 (1974b).

Henry Bokuniewicz, personal communication; School of Marine and Atmospheric Science, Stony Brook University, NY.

Charles Flagg, personal communication; School of Marine and Atmospheric Science, Stony Brook University, NY.

National Buoy Data Center; National Oceanic and Atmospheric Administration. Accessed June, 2008. http://www.ndbc.noaa.gov/

United States Geological Survey. Accessed June 2008.
http://waterdata.usgs.gov/nwis
School of Marine and Atmospheric Science; Stony Brook University. Accessed June, 2008. http://lishore.org/

National Climatic Data Center; National Oceanic and Atmospheric Administration. Accessed June, 2008. http://cdo.ncdc.noaa.gov/qclcd/QCLCD

Appendix

Figure 1. Station locations. Diamonds – SeaCats, Blue - SeaCats used; Squares – Water Level Stations; Circle - Buoy 44017; Stars – MET stations.

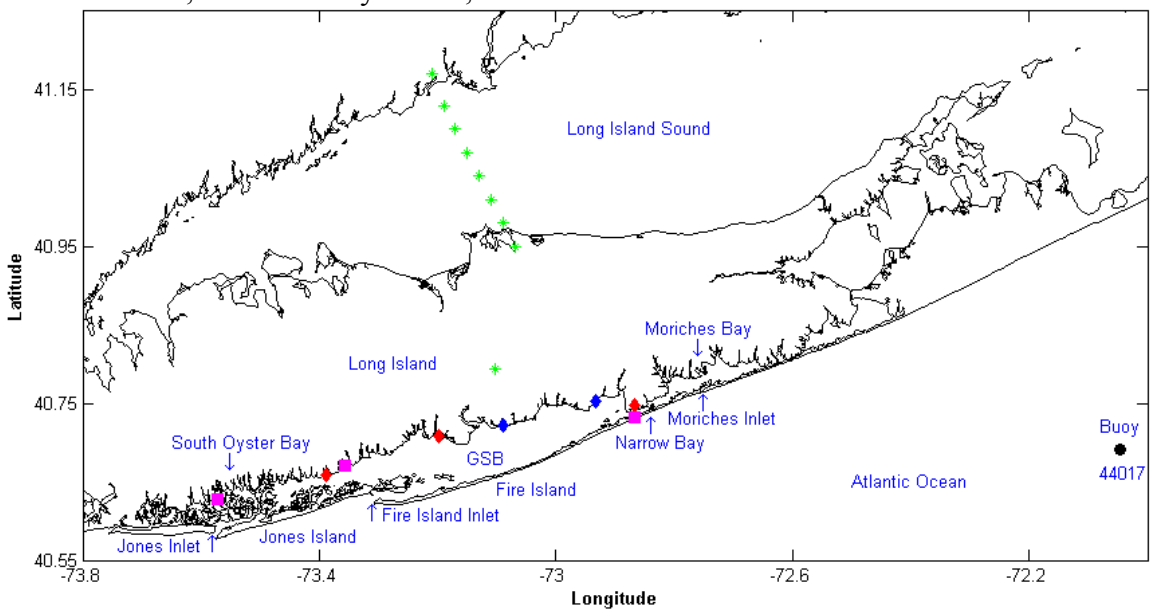

Figure 2. Hard clam landings since 1960 in thousands of bushels. Modified from NYDEC.

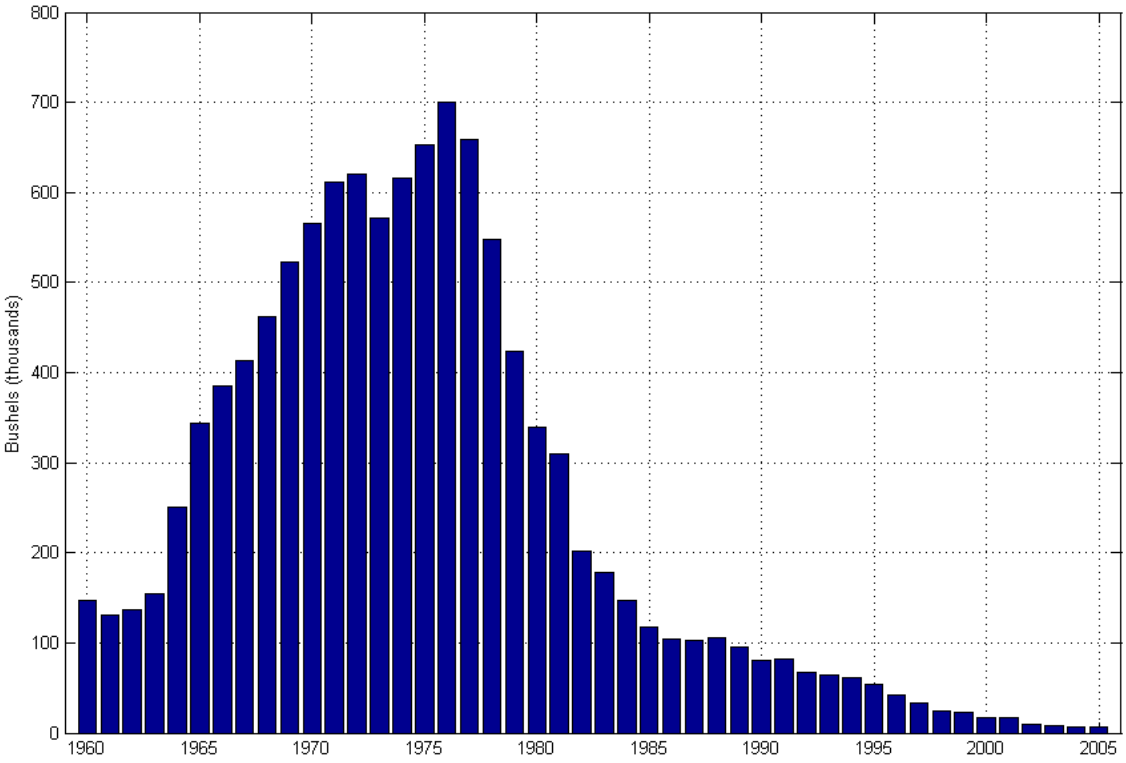

Figure 3. Temperature records for 2007 at Bellport and Blue Point

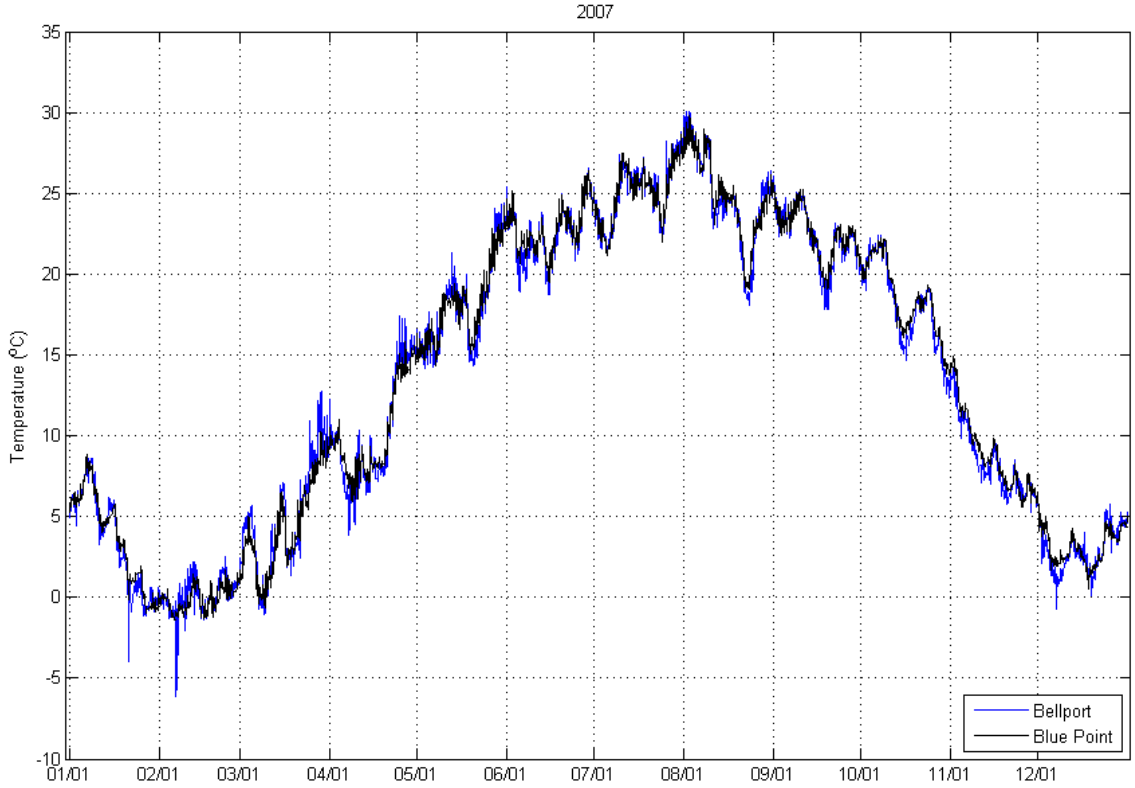

Figure 4. Temperature records including Tanner Park for 2007.

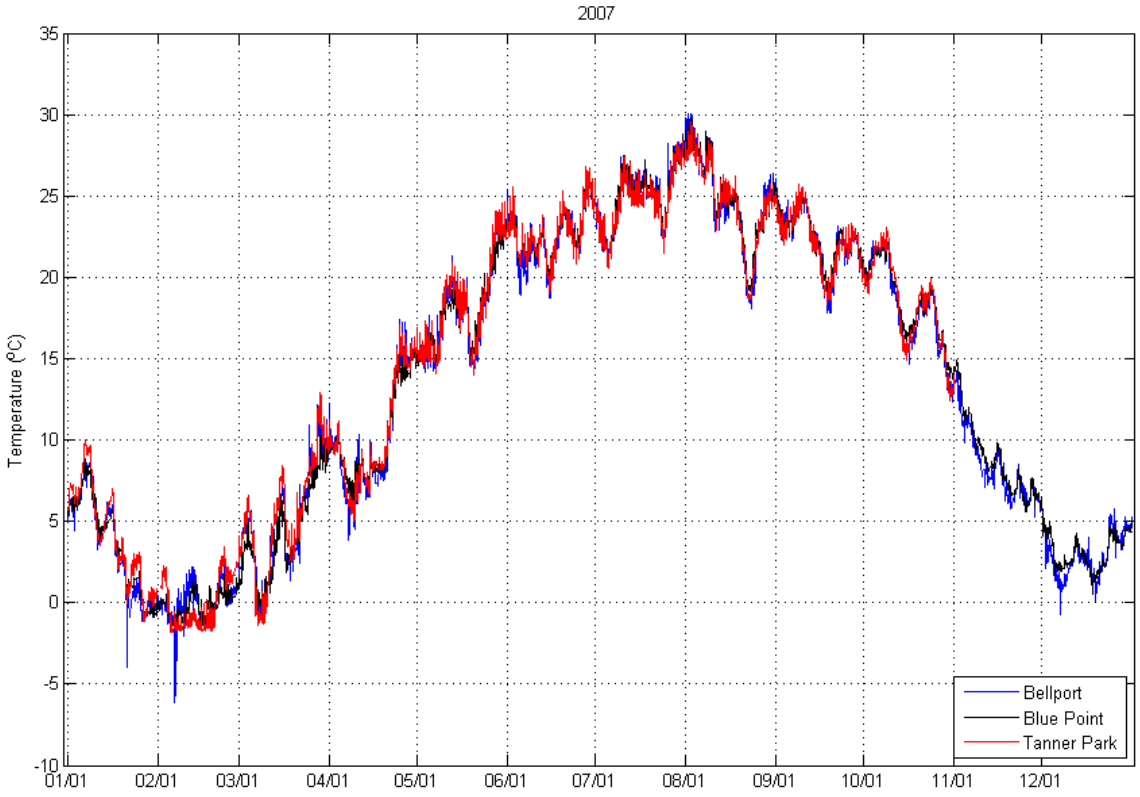

Figure 5. Salinity records at Bellport and Blue Point for 2007.

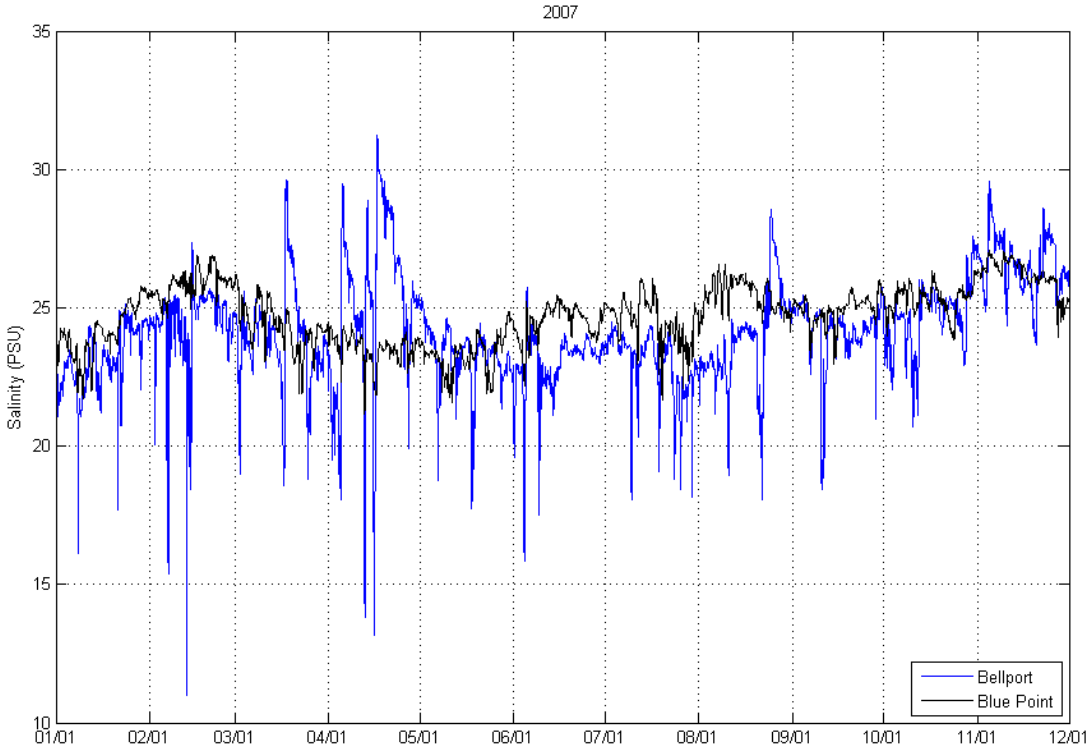

Figure 6. Salinity records at Bellport and Blue Point for September 2007.

Figure 7. Wind vectors at 10% magnitude for September 2007.

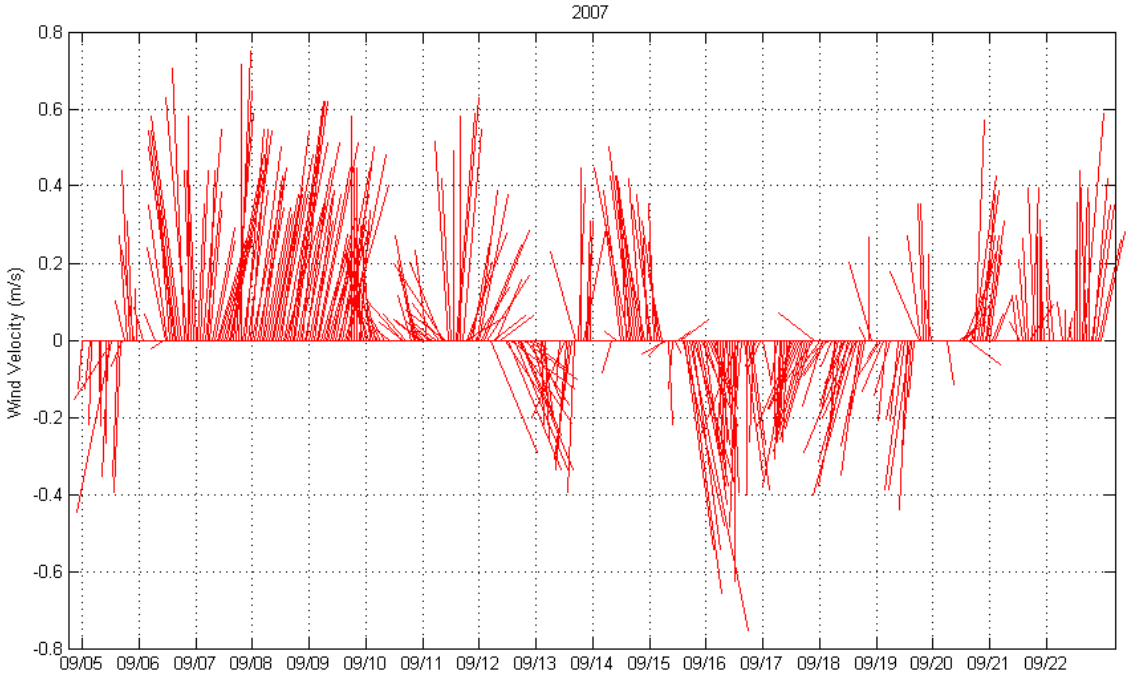

Figure 8. Air, Ocean, and Bay temperature records for 2007. 30 day filter.

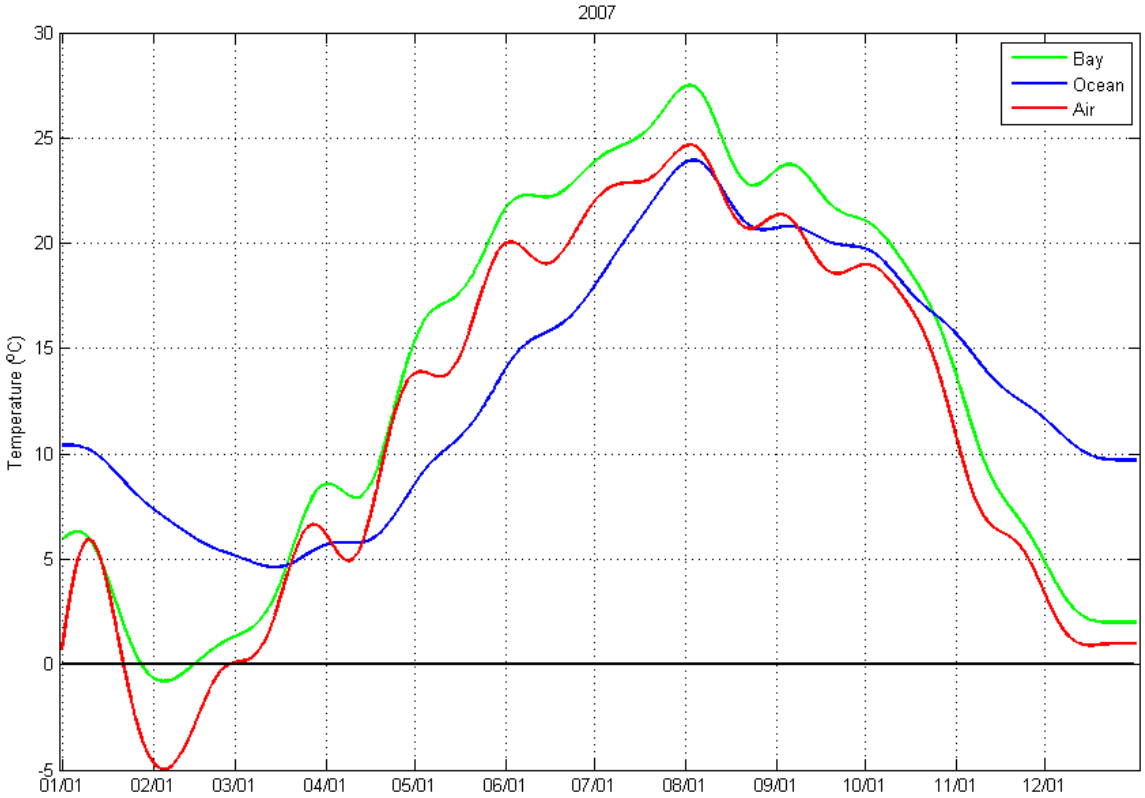

Figure 9. Net, Shortwave, Sensible, Latent, and Longwave heat fluxes for 2007. 30 day filter.

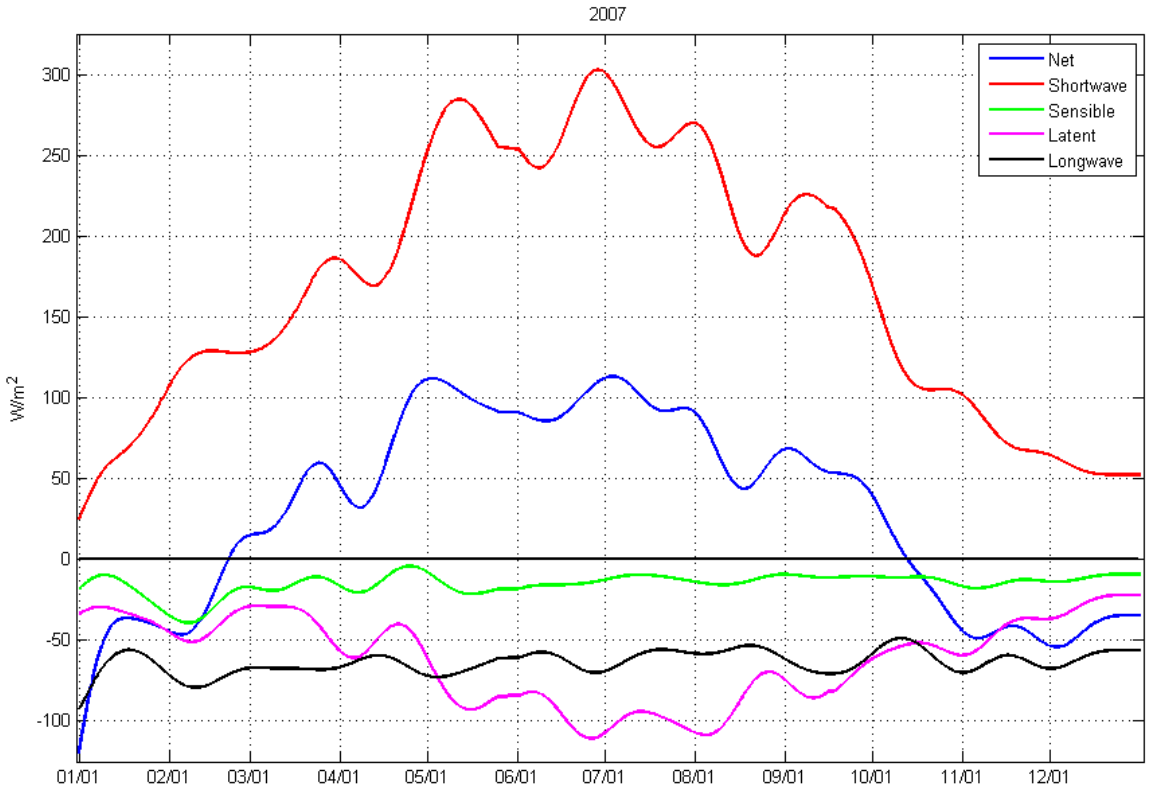

Figure 10. Bay temperature and latent heat flux. 30 day filter.

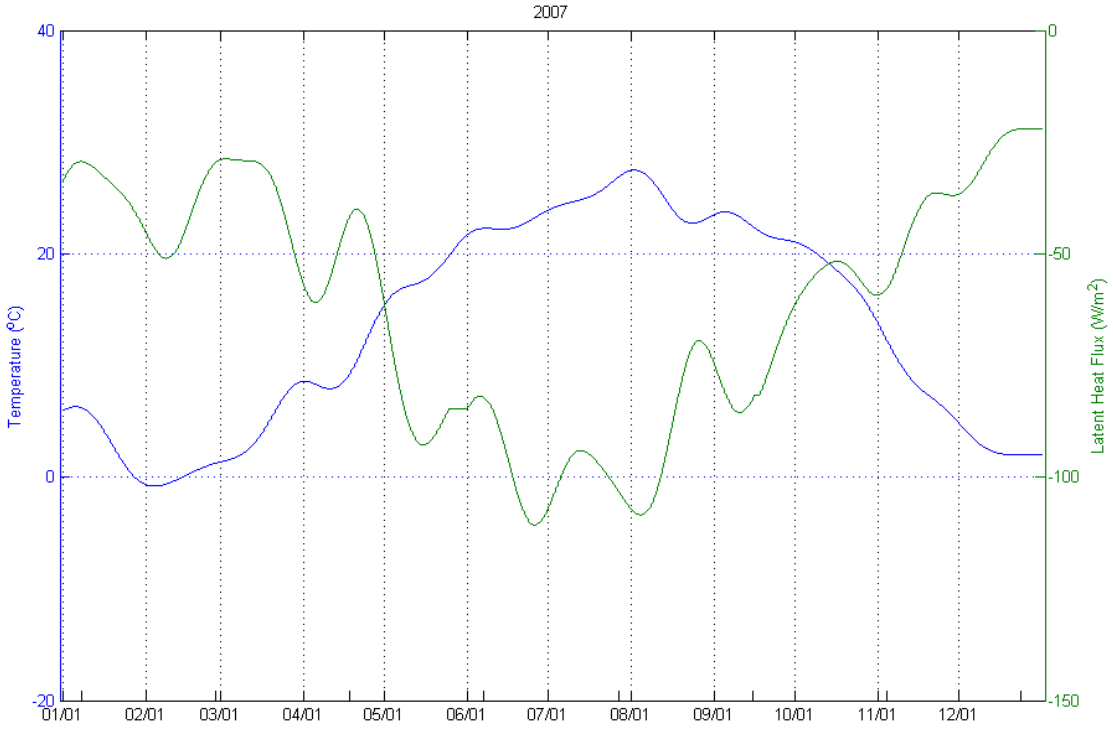

Figure 11. Time rate of change of thermal energy and the temperature and volume components. 30 day filter.

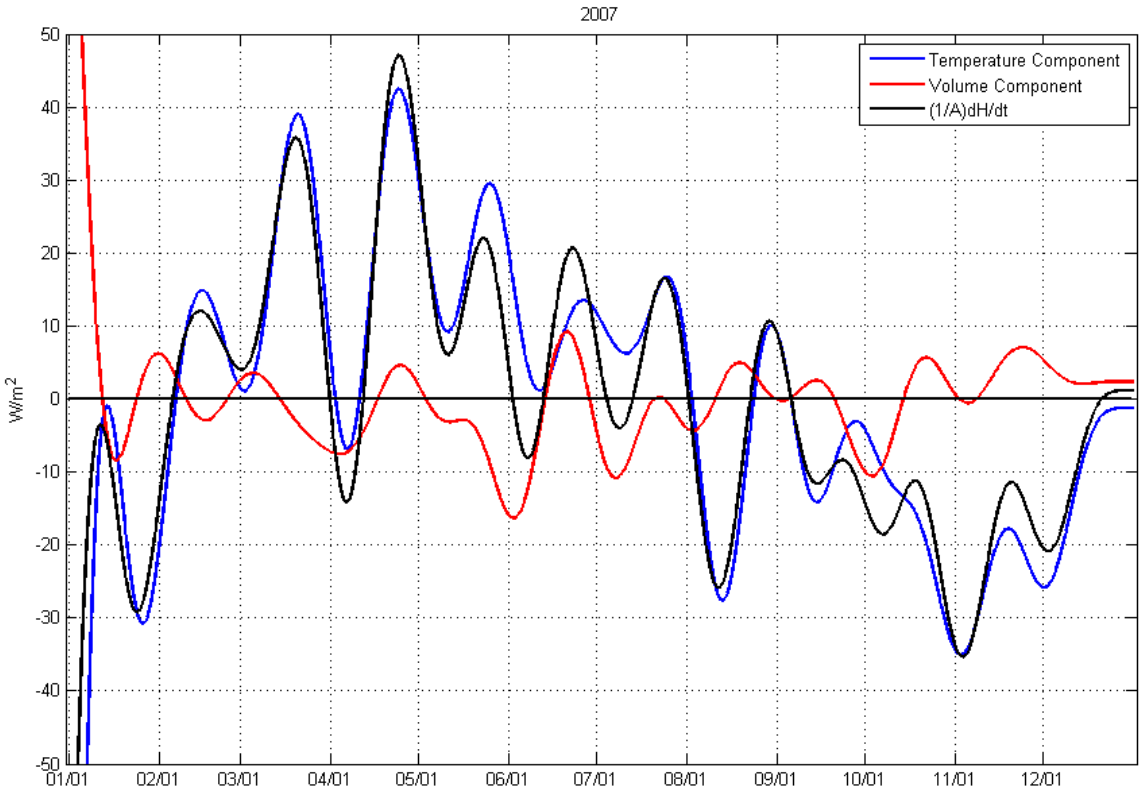

Figure 12. Surface heat flux, time rate of change of thermal energy, and indirect boundary flux. 30 day filter.

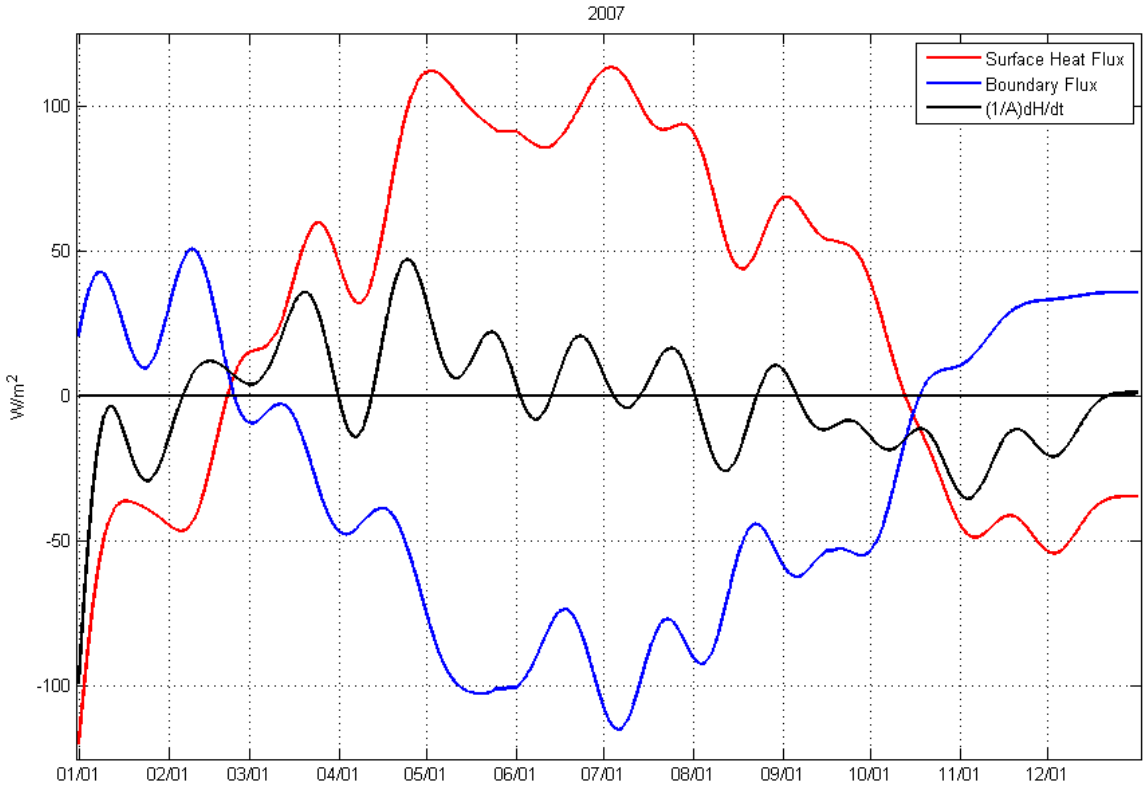

Figure 13. Terms IV through VII and the direct boundary flux. 30 day filter.

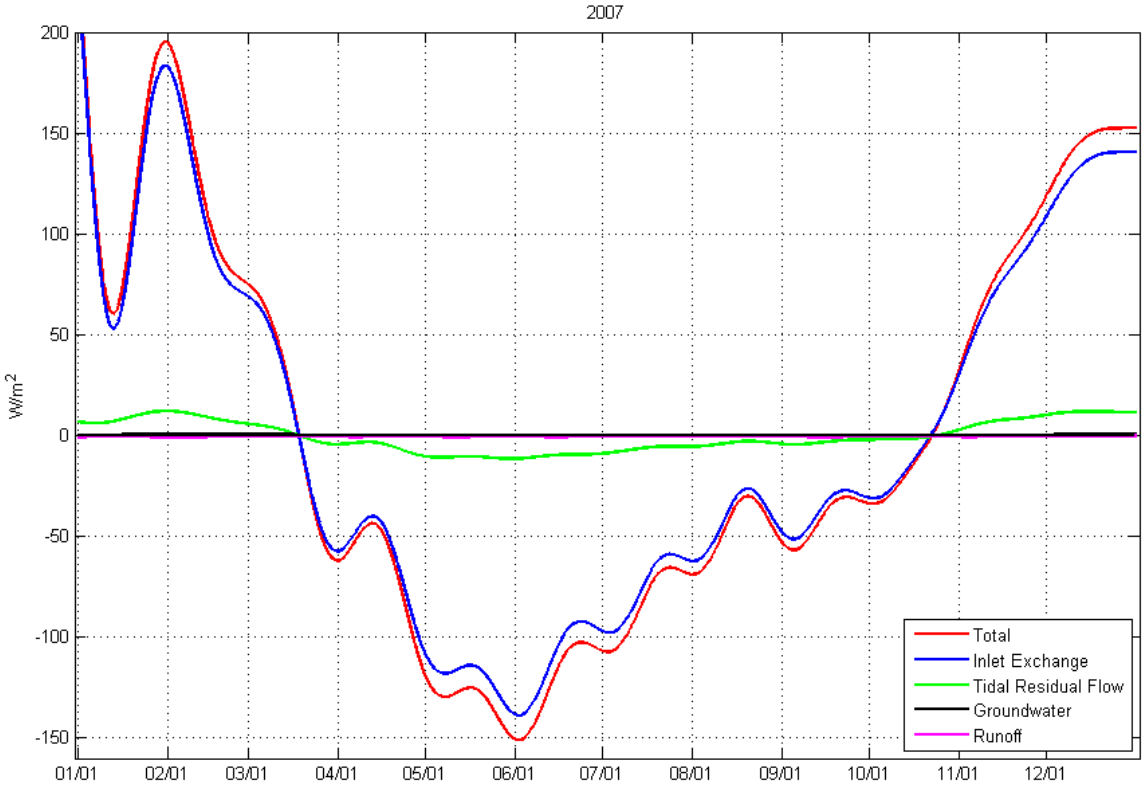

Figure 14. Bay, ocean, and air temperature for September 2007.

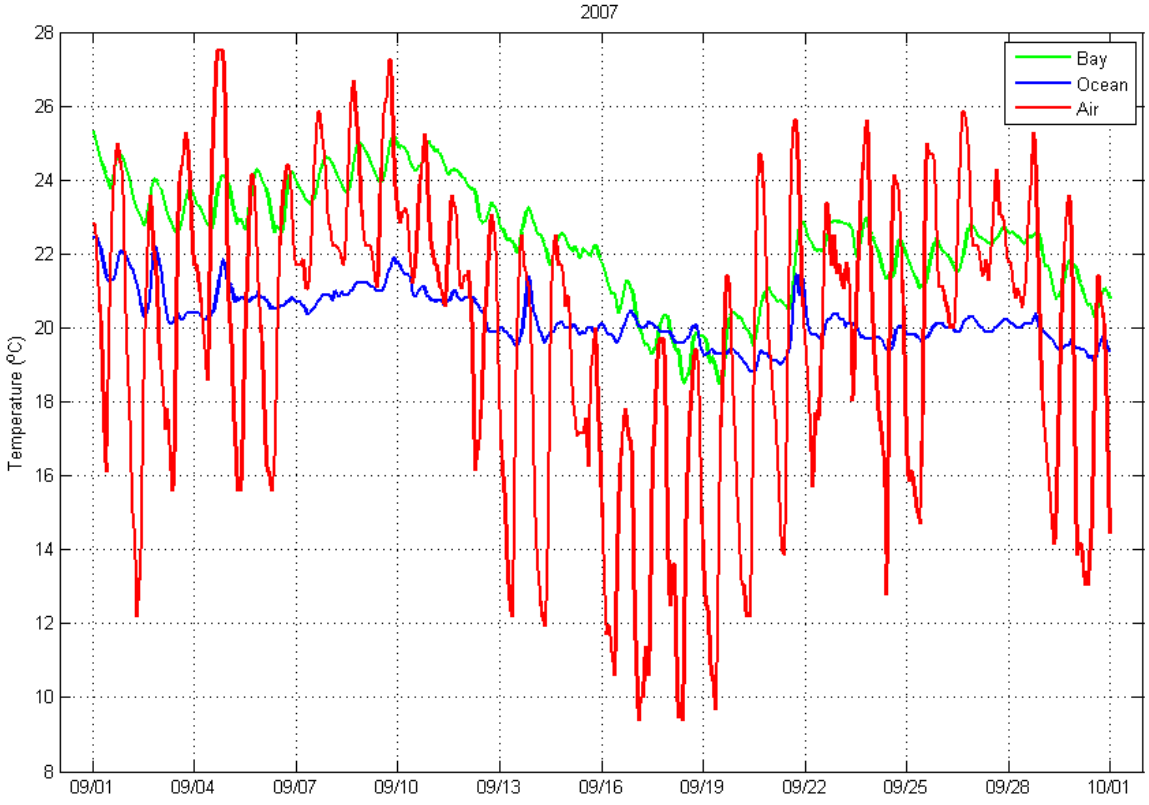

Figure 15. Cloud cover, air pressure, and precipitation for September 2007. Red line indicates a synoptic scale storm event.

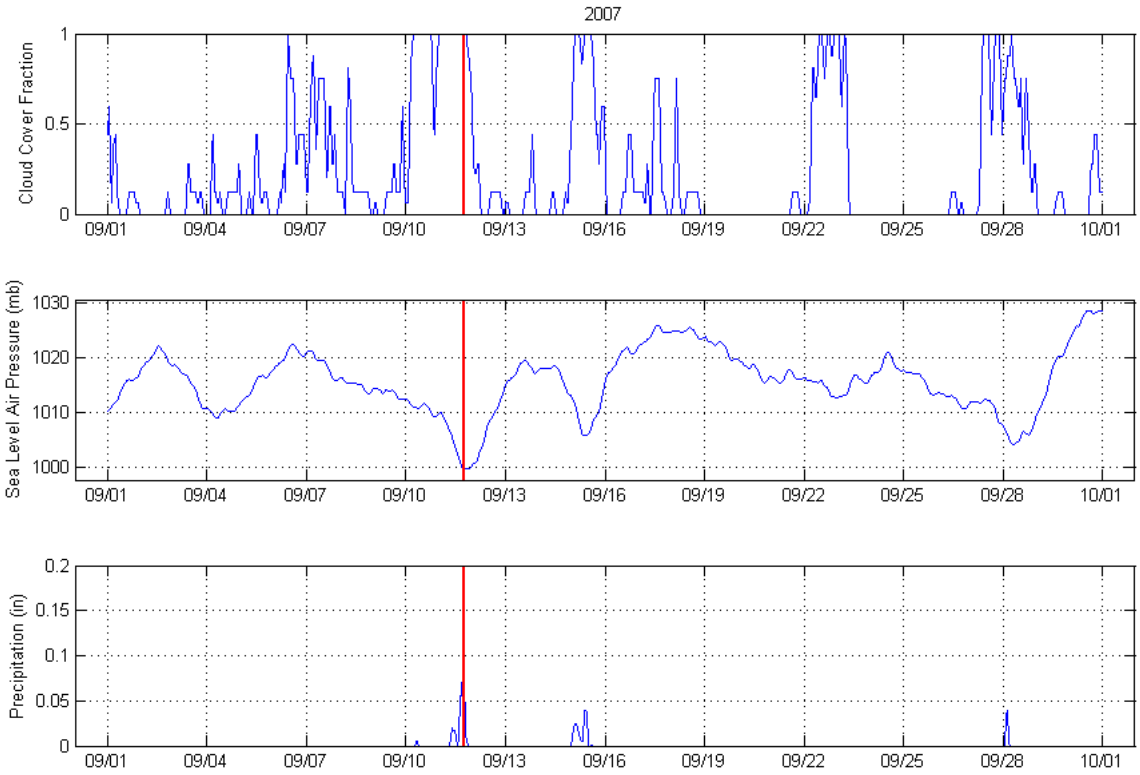

Figure 16. Surface heat fluxes for September. Red line indicates a synoptic scale storm event. * - missing data. 48 hour filter.

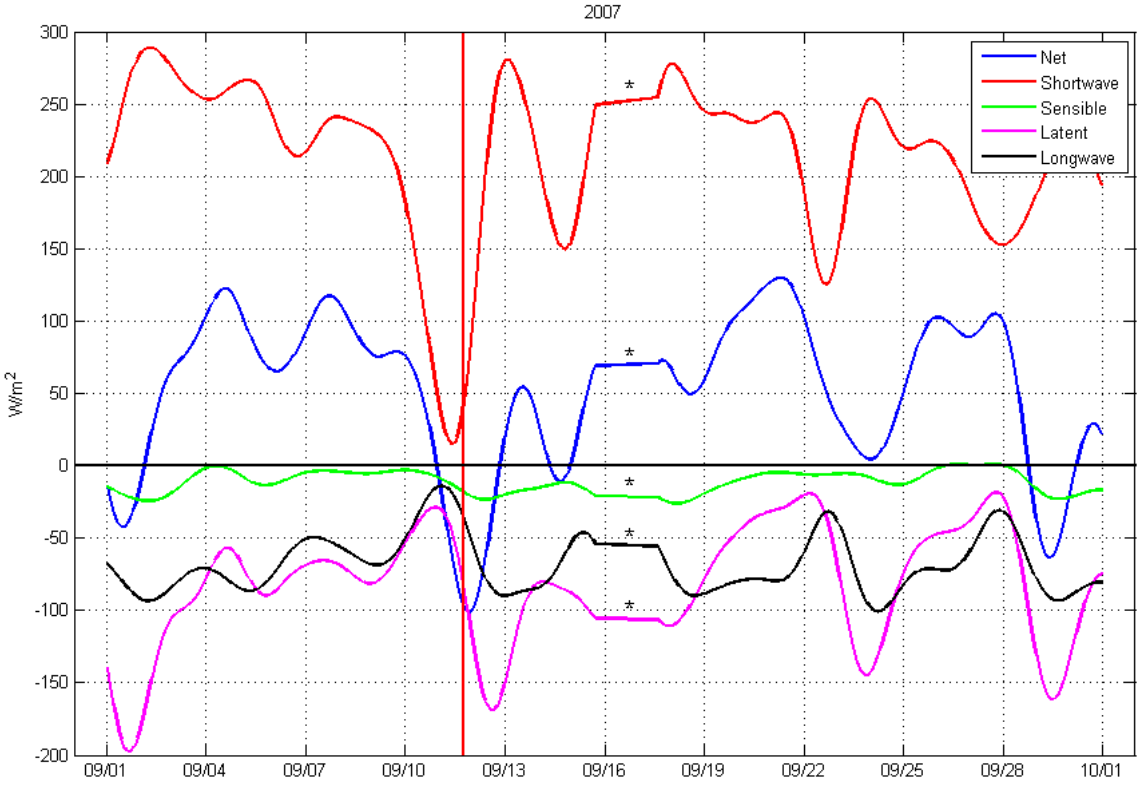

Figure 17. Time rate of change of thermal energy in the bay for September. Red line indicates a synoptic scale storm event. 48 hour filter.

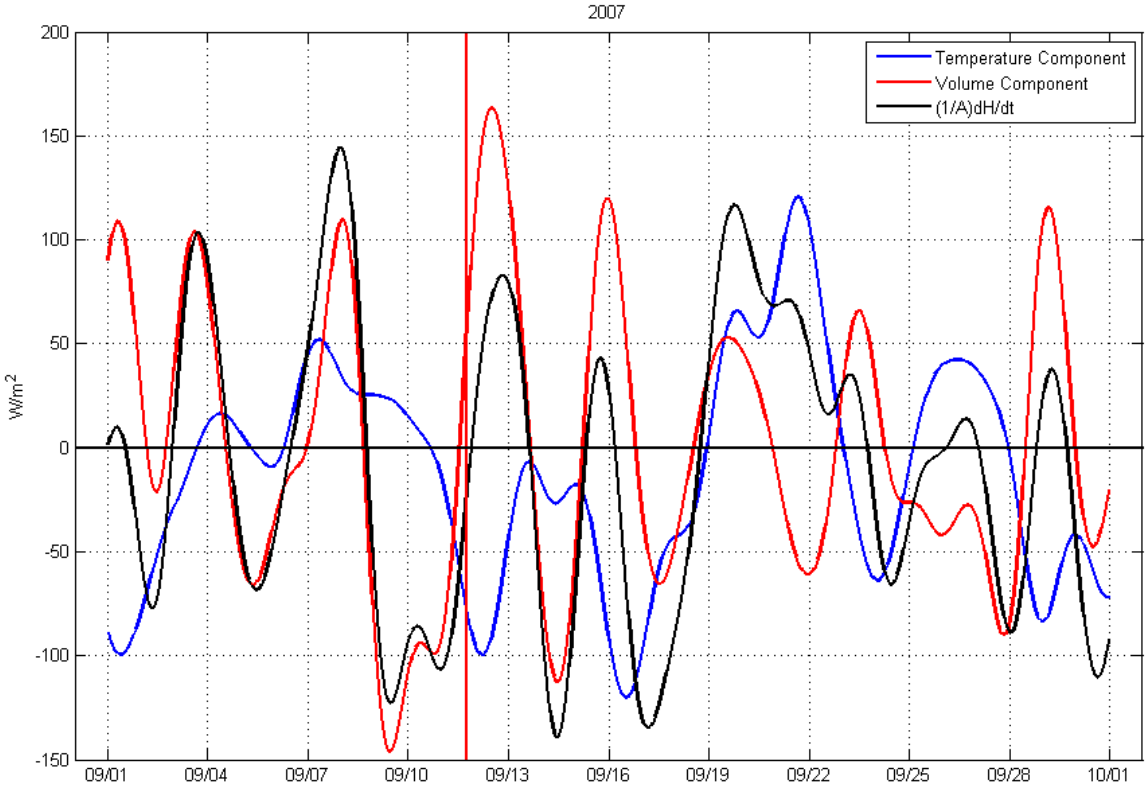

Figure 18. Direct boundary flux with submarine groundwater discharge (Q_g) increased by two orders of magnitude, from 2.5 m^3 s^{-1} to 500 m^3 s^{-1}. 30 day filter.

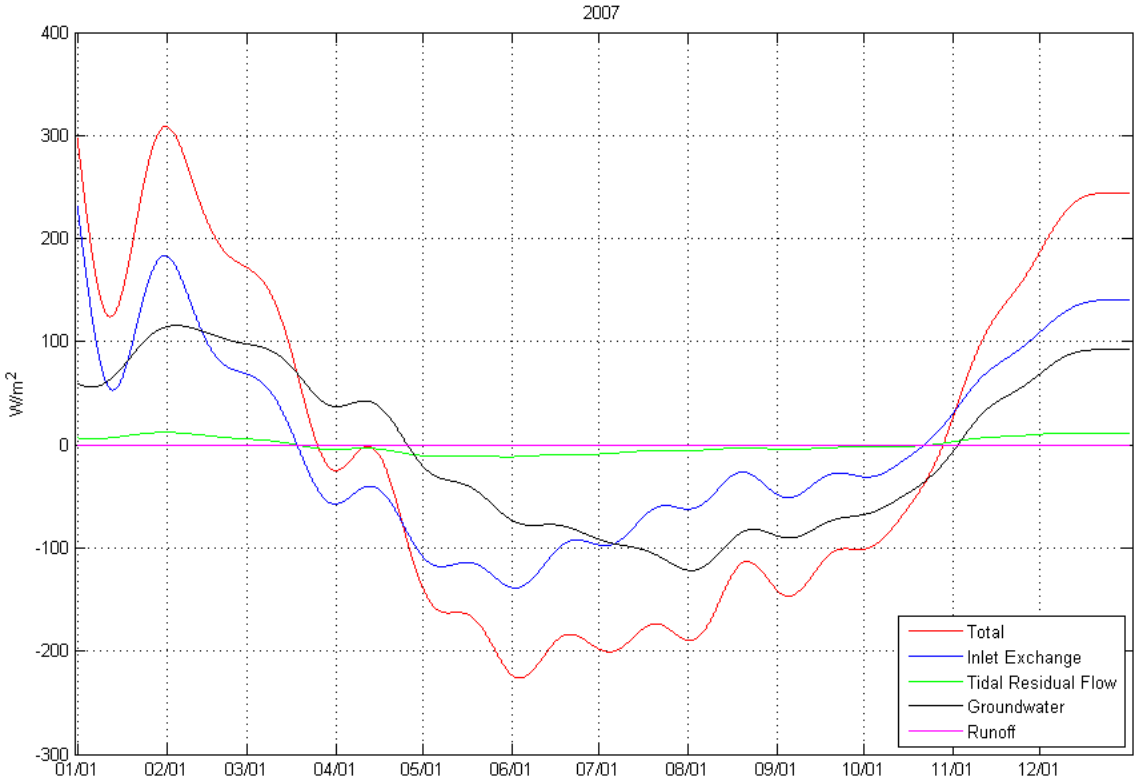

Figure 19. Comparison of the indirect boundary flux and direct boundary flux. 30 day filter.

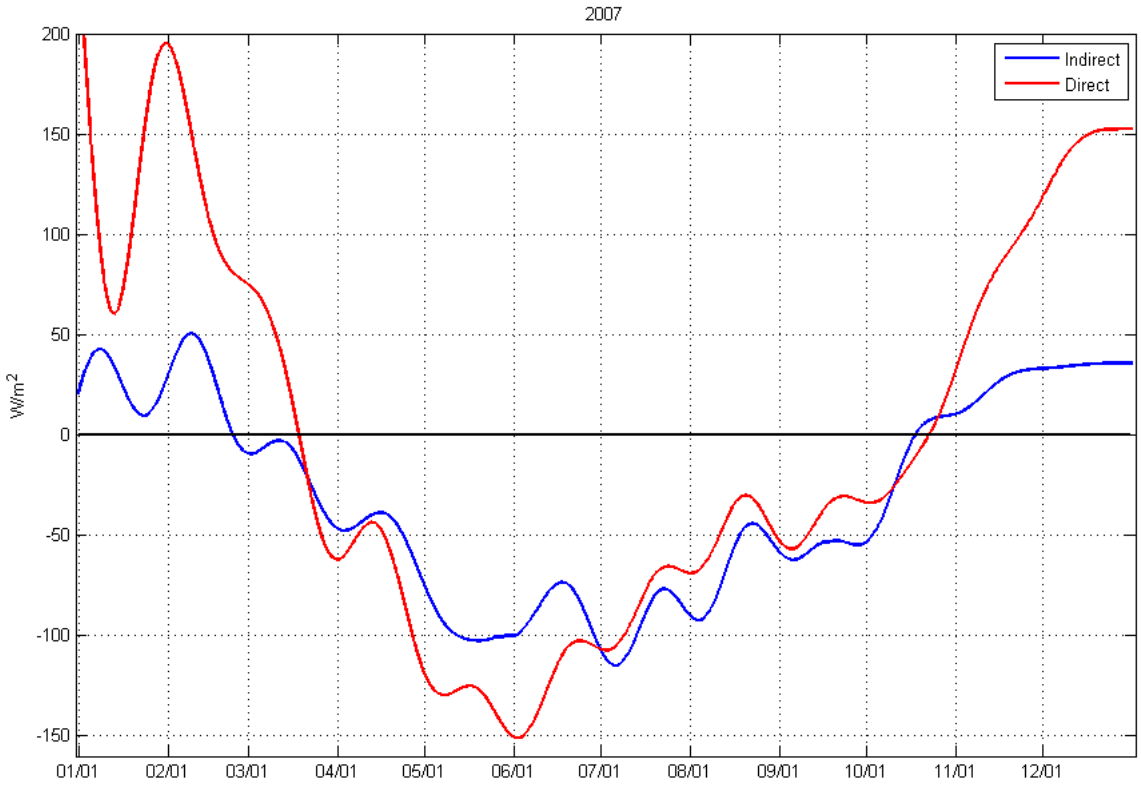

Figure 20. Indirect boundary flux and ocean-bay temperature difference. 30 day filter.

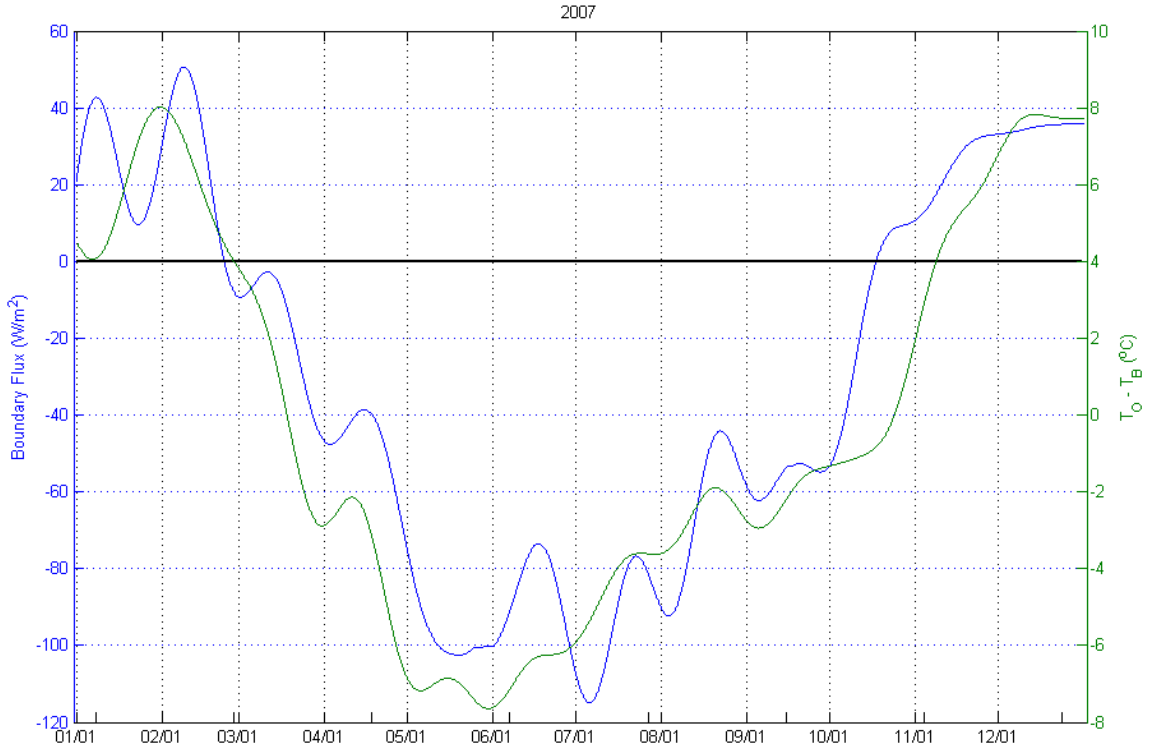

Figure 21. Direct boundary flux and ocean-bay temperature difference. 30 day filter.

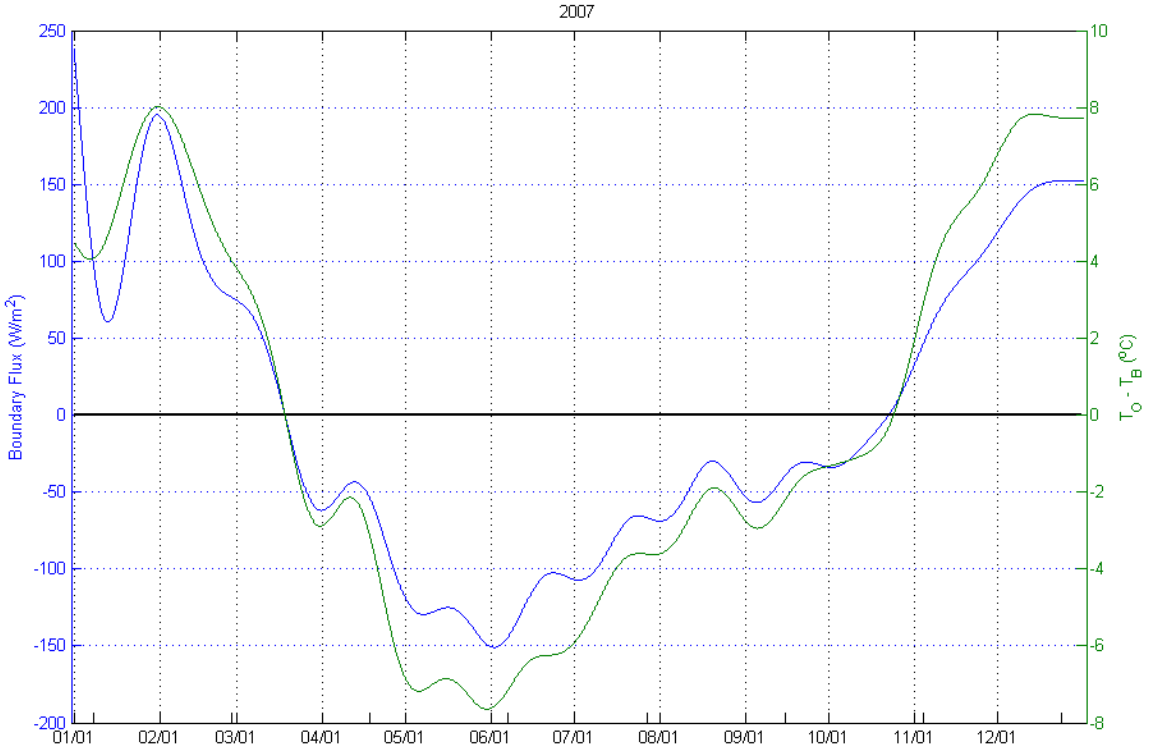

Figure 22. Change in variance with change in alpha.

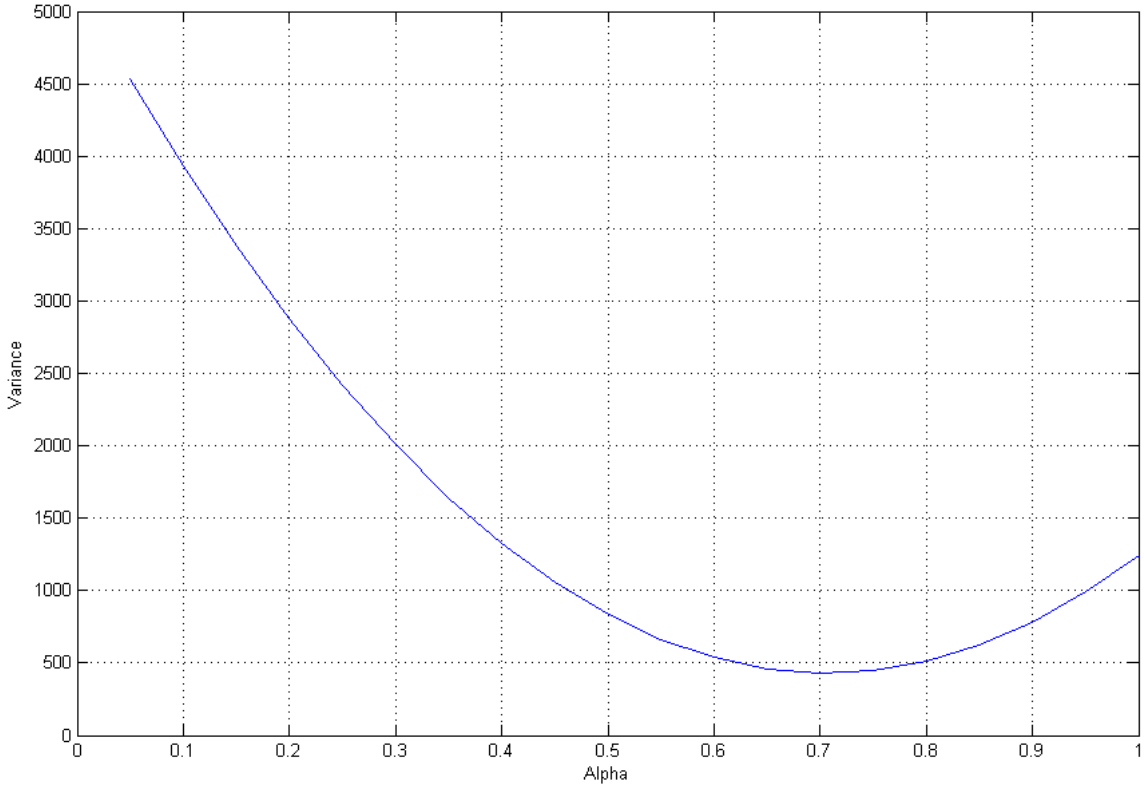

Figure 23. Comparison of the indirect boundary flux and direct boundary flux with recirculation of 70%, including previous direct boundary flux with 100% mixing. 30 day filter.

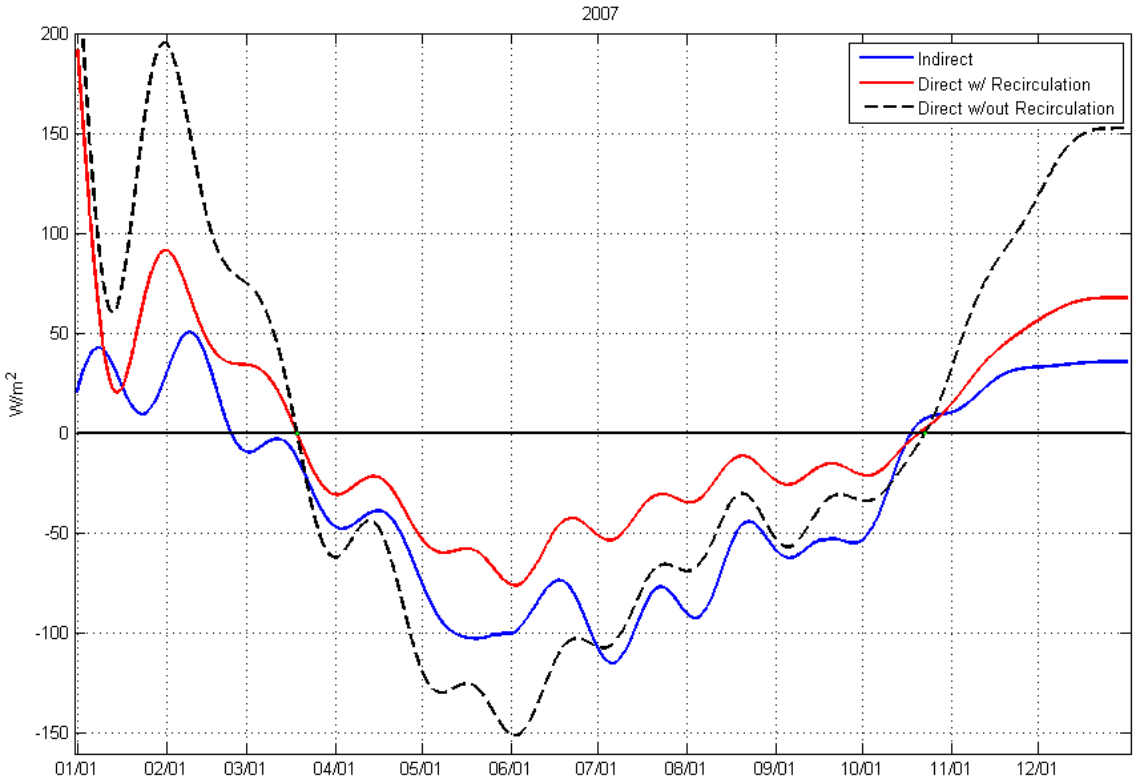

Figure 24. Direct boundary flux with recirculation at 70% for September 2007. Red line indicates a synoptic scale storm event. 48 hour filter.

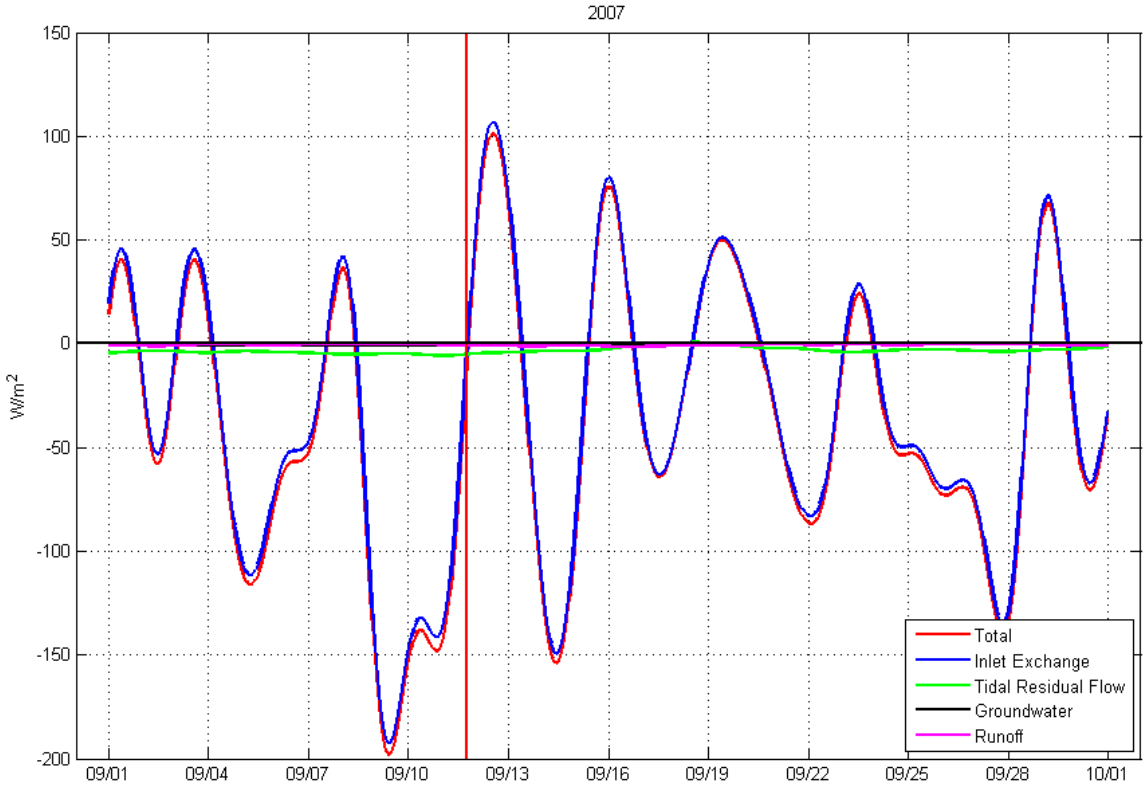

Figure 25. Net surface heat flux and the temperature component of the time rate of change of thermal energy. Red line indicates a synoptic scale storm event. * - missing data. 48 hour filter.